One-Loop Soft Anomalous Dimension Matrices for $t\bar{t}j$ Hadroproduction

B. Chargeishvili, M. V. Garzelli, S.-O. Moch

II. Institut für Theoretische Physik, Universität Hamburg

One-loop soft anomalous dimension matrices for $t\bar{t}j$ hadroproduction

Bakar Chargeishvili, Maria Vittoria Garzelli, Sven-Olaf Moch

II. Institut für Theoretische Physik, Universität Hamburg, Luruper Chaussee 149, D – 22761 Hamburg, Germany

ABSTRACT

We calculate the one-loop corrections to the soft anomalous dimension matrices for the production of a top-antitop quark pair in association with a jet at hadron colliders. This is a step forward towards implementing a procedure for the resummation of soft-gluon emission logarithms for the $t\bar{t}j + X$ hadroproduction process, that will enable the improvement of the accuracy of the $t\bar{t}j + X$ cross sections, beyond the current degree of knowledge. The latter, so far, has reached the next-to-leading order (NLO) level, complemented by the accuracy of the Shower Monte Carlo approaches used in matching the NLO computations to parton showers (PS) and by merging with matrix elements with a different number of light jets.

1

1 Introduction

Studying $t\bar{t}j + X$ production at hadron colliders is one of the relevant projects for better understanding top-quark physics. Already some years ago, it was shown that the differential cross sections for $t\bar{t}j + X$ hadroproduction with respect to the observable $\rho_s = 2\,m_t\,/\sqrt{s_{t\bar{t}j}}$ introduced in Ref. [1], where m_t is the top-quark mass and $s_{t\bar{t}j}$ is the squared invariant mass of the system of the top, antitop quarks and hardest jet, shows a good sensitivity to the top-quark mass value and hence can be used for its determination. The ATLAS and CMS collaborations obtained the top-quark mass from the normalized ρ_s distribution at $\sqrt{S}$ = 8 TeV [2,3], following a first analysis by ATLAS at $\sqrt{S}$ = 7 TeV [4,5], which served as a proof-of-concept of the methodology. Further top-quark mass extractions at $\sqrt{S}$ = 13 TeV are currently in preparation and/or in a preliminary status [6], also thanks to the most recent high-statistics data on single- and multi-differential cross sections collected during Run 2 at the Large Hadron Collider (LHC). A summary of most of the measurements of top-quark mass already performed by the ATLAS and CMS collaborations, using this and other methods, can be found in e.g. Ref. [7].

Measurements relying on the comparison between Quantum Chromodynamics (QCD) predictions for (differential) cross sections with a well-defined accuracy and experimental data, like those mentioned above, are prominent examples of the so-called indirect methods for determining the top-quark mass. They have become clear competitors to the direct measurements, based on the kinematical reconstruction of top quarks from their decay products with the aid of Monte Carlo event generators, and provide the advantage, with respect to the latter, of leading to mass values in various well-defined mass renormalization schemes, used for computing the cross section itself. Beside the value of the pole mass, the values of the short-distance masses like the $\overline{\text{MS}}$ [8], and the MSR one [9,10], intrinsically more precise because insensitive to long-distance physics effects, can be extracted [11]. At present, top-quark mass extractions via the $t\bar{t}j + X$ process are based on next-to-leading-order (NLO) QCD estimates of the corresponding production cross sections. The NLO QCD corrections to $pp \rightarrow t\bar{t}j$ production were first calculated in Ref. [12]. Uncertainties due to missing higher orders accompanying the NLO QCD cross sections, translate into uncertainties on the m_t value amounting to $\sim \pm 0.5$ GeV in the most recent analyses [6]. It is expected that elevating cross section accuracy beyond NLO could improve the current indirect estimates of the top-quark mass, leading to reduced systematic uncertainties. On the other hand, issues in the comparison between detailed experimental data already available and state-of-the-art theory predictions with an accuracy not matching the one of the data and, thus, requiring further improvements, have already been pointed out in case of multi-differential cross sections for the $t\bar{t}$ production case (see e.g. Ref. [13]).

While NLO QCD computations of $t\bar{t}j$ hadroproduction were matched to parton shower approaches using various methods [14–17], approximate NLO electroweak corrections were estimated [18], and merging with $t\bar{t}$ computations was also implemented [18,19] using fully numerical methods, the extension of the accuracy of both the total and differential cross sections to the next-to-next-to-leading-order (NNLO) in QCD still represents significant technical challenges [20]. At NNLO these consist of the two-loop integrals entering into

double virtual contributions, which are mostly unknown for $2 \rightarrow 3$ kinematics with massive partons, as well as approaches to deal with the singularities arising from the soft and collinear emissions of massless particles and with the cancellation of the corresponding infrared poles, which also need further development.

Meanwhile, in conjunction with the already available amplitudes at LO and NLO, it is possible to employ the well-established formalism of resummation [21, 22] of large logarithmic terms associated to soft-gluon emission, to predict the all-order contribution coming from this specific class of higher-order terms. This class provides the dominant contribution to the cross section in the phase-space regions where the corresponding terms are particularly large, i.e. close to threshold. By re-expanding the all-order results with a well defined logarithmic accuracy (leading logarithmic, next-to-leading logarithmic, etc.), it is then possible to determine differential cross sections with different degrees of approximate fixed-order accuracy. In particular, approximate NNLO differential cross sections for the $t\bar{t}j$ hadroproduction process might be obtained for the first time. One may foresee a scientific development somehow similar to the one for the $t\bar{t} + X$ hadroproduction process, where, historically, approximate NNLO predictions for total cross sections [23] were published before exact NNLO results could be computed [24–27]. The main difference with respect to the $t\bar{t} + X$ hadroproduction process is that, while for the latter it was possible to first develop calculations for total inclusive cross sections and check the validity of the threshold approximation, predictions for the $t\bar{t}j + X$ hadroproduction process are divergent already at leading order, implying the necessity to impose fiducial cuts on the light jet and work at the differential level from the very beginning.

To be able to successfully apply the resummation formalism at the next-to-leading logarithmic (NLL) level, one of the missing ingredients are the one-loop corrections to the soft functions, that enter the formulas used to refactorize partonic cross sections in the framework of the resummation formalism of soft-gluon logarithms. In the following of this manuscript, we define the soft functions for $t\bar{t} + \text{jet}$ production in parton-parton scattering and express them in terms of their building blocks, the soft anomalous dimension matrices in Section 2. We provide the details of the calculation of the latter at 1-loop and the procedure to automatize this step in Section 3. We report the analytic results of this calculation in Section 4. We discuss their connection with the infrared pole structure of the virtual amplitudes and related cross-checks in Section 5. We draw our conclusions in Section 6. Technical details on the color bases and the derivation of the color structures of the soft anomalous dimension matrices are left to the Appendices. Beyond the specific application on which we focused in this work, a review of the status of calculations and explicit results on soft anomalous dimension matrices for a number of processes interesting for collider phenomenology appeared recently in Ref. [28]. A general recipe for the calculation of the color structures of these matrices can be found in Ref. [29]. On the other hand, recent developments on the calculation of soft anomalous dimension matrices in multi-particle scattering amplitudes at higher orders are summarized in Ref. [30], together with up-to-date insights and perspectives for the future.

3

2 Definition of the soft function for $t\bar{t}j$ hadroproduction

Factorization theorems allow to express partonic cross sections (or partonic multi-particle scattering amplitudes) in terms of hard functions, soft functions and jet functions. Emissions that are neither soft, nor collinear, are included in the hard functions, collinear non-soft emissions are encoded in the jet functions and soft wide-angle (i.e. non-collinear) emissions are described by the soft functions. The latter kind of emissions are conveniently parametrized by Wilson lines. Adopting the notation of Ref. [31], a general Wilson line is defined along the path $\mathcal{C}$ in space-time, beginning at the point z^μ and ending at the point z'^μ:

$$W^{(f)}\left[\mathcal{C}; z', z\right] = \mathcal{P} \exp\left[-ig \int_{\eta_1}^{\eta_2} d\eta \, \frac{dy(\eta)}{d\eta} \cdot A^{(f)}(y(\eta))\right], \tag{1}$$

where g is the $\mathrm{SU}(N_c)$ gauge coupling, with N_c equal to the number of colors, $A_\mu^{(f)}(y)$ is the gauge field in the fundamental or adjoint representation of the $\mathrm{SU}(N_c)$ group, corresponding to f being a quark or a gluon, respectively, and $\mathcal{P}$ denotes path-ordering in the same sense of η, i.e. when the exponential is expanded, the fields with the higher value of η are on the left. The path $\mathcal{C}$ is parametrized by a function $y^\mu(\eta)$ in the variable η, with endpoints $y^\mu(\eta_1) = z^\mu$ and $y^\mu(\eta_2) = z'^\mu$. The classical trajectory of an initial or final state parton moving with velocity β^μ can be expressed as a straight line $y^\mu(\eta) = \eta\beta^\mu + x^\mu$, stretching from the interaction vertex x^μ to infinity, either from the distant past (initial state, $\eta_1 = -\infty$) or towards the distant future (final state, $\eta_2 = +\infty$). The corresponding Wilson line is given by

$$\Phi_\beta^{(f)}(\eta_2, \eta_1; x) = \mathcal{P} \exp\left[-ig \int_{\eta_1}^{\eta_2} d\eta \, \beta \cdot A^{(f)}(\eta\beta + x)\right]. \tag{2}$$

The $t\bar{t}j$ hadroproduction process has the following structure at the Born level:

$$a(\beta_a, c_a^{(f_a)}) \; b(\beta_b, c_b^{(f_b)}) \to 1(\beta_1, c_1^{(f_1)}) \; 2(\beta_2, c_2^{(f_2)}) \; 3(\beta_3, c_3^{(f_3)}), \tag{3}$$

where $c_i^{(f)}$ are color indices in the representation f described above, depending on the kind of parton i under consideration. In particular, $t\bar{t}j$ hadroproduction at the LHC can occur through distinct tree-level hard-scattering subprocesses (see Eq. (13) in the following). For each of the two subprocesses $gg \to t\bar{t}g$ and $q\bar{q} \to t\bar{t}g$, it is useful to choose a color basis $\{\mathbf{c}_I\}$, with the index I labeling a generic element of the color basis, and to define a set of eikonal non-local operators $\{\omega_I\}$, in one by one correspondence with the elements of the color basis. We emphasize that the color basis for a specific subprocess is not unique and depends on the kinds of partons (quarks, antiquarks and gluons) involved in the subprocess. In Mellin space we write the ω_I operator as

$$\omega_I^{\{f\}}(x)_{\{c_k\}} = \sum_{d_i} \; \Phi_{\beta_3}^{f_3}(\infty, 0; x)_{c_3, d_3} \Phi_{\beta_2}^{f_2}(\infty, 0; x)_{c_2, d_2} \Phi_{\beta_1}^{f_1}(\infty, 0; x)_{c_1, d_1} \left(\mathbf{c}_I^{\{f\}}\right)_{d_3 d_2 d_1, d_b d_a}$$

$$\times \Phi_{\beta_a}^{f_a}(0, -\infty; x)_{d_a, c_a} \Phi_{\beta_b}^{f_b}(0, -\infty; x)_{d_b, c_b}, \tag{4}$$

which generalizes the expression used in Ref. [31] for the dijet case to our process. In the previous formula the color tensor $\left(\mathbf{c}_I^{\{f\}}\right)_{d_3 d_2 d_1, d_b d_a}$ links the five Wilson lines corresponding

to the external legs of the subprocess and encodes the coupling of the Wilson lines one with each other in color space, while the superscript $\{f\}$ refers to the ensemble of the flavors of all external lines, i.e. $\{f_a, f_b, f_1, f_2, f_3\}$. In terms of this operator the eikonal cross section is given by [32, 33]:

$$\sigma_{LI}^{\{f\},\text{eik}}(\alpha_s, \epsilon) = \sum_\xi \delta(w - w(\xi)) \times \left\langle 0 \left| \overline{T} \left[\left(\omega_L^{\{f\}}(0) \right)^\dagger_{\{b_i\}} \right] \right| \xi \right\rangle \left\langle \xi \left| T \left[\omega_I^{\{f\}}(0)_{\{b_i\}} \right] \right| 0 \right\rangle, \quad (5)$$

where T and $\overline{T}$ are time ordering and anti-time ordering operators respectively, $|\xi\rangle$ denotes a set of intermediate states, L is an index running over the elements of the color basis, analogously to I, and $\alpha_s = g^2/(4\pi)$ is the strong coupling constant. The contribution of the $|\xi\rangle$-state to the weight is given by $w(\xi)$, where w is the corresponding measure of the eikonal phase space near partonic threshold in the center–of–mass frame of the colliding partons [31]. In the eikonal approximation of Eq. (5) soft gluons are allowed to be collinear as well. Dimensional regularization is understood, according to which we work in D dimensions, with $D = 4 - \epsilon$, and soft and soft-collinear singularities are re-expressed in terms of poles for $\epsilon \to 0$. In the definition of the soft function adopted here, we have to factor out the soft-collinear contributions, since only soft wide-angle emissions are included[1]. Thus, the soft function is defined as the part free of collinear divergences of the eikonal cross section, introduced in Eq. (5), after a Mellin transform of the latter, which leads to the following factorized form

$$\sigma_{LI}^{\{f\},eik^N} = S_{LI}^{\{f\}} \, ^N j_a^N j_b^N j_1^N j_2^N j_3^N \, . \quad (6)$$

In this formula the superscript N indicates that the N-th Mellin moment of the cross section is obtained through the transform, S^N denotes the soft-function matrix in Mellin space, whereas j_a^N, j_b^N, j_1^N, j_2^N, j_3^N are the jet functions corresponding to the initial- and final-state particles, describing both collinear soft and collinear non-soft emissions.

Notice that, due to this definition, if we expand in a power series the exponentials which come from the Wilson lines involved in the soft-function construction, at the Born level, where there is no need for renormalization, we simply get

$$S_{LI}^{\{f\},0} = \left\langle \mathbf{c}_L^{\{f\}} | \mathbf{c}_I^{\{f\}} \right\rangle . \quad (7)$$

To be able to perform the resummation of the logarithms associated to soft wide-angle gluon emissions and see how the soft function exponentiates, we have to study its renormalization properties. By definition, each soft function is free of collinear divergences. However, it still contains the ultraviolet (UV) divergences, which can be re-expressed in terms of poles for $\epsilon \to 0$ through dimensional regularization. Then the UV poles have to be renormalized using appropriate counter-terms. In the $\overline{\text{MS}}$ scheme these counter-terms contain the UV divergent part of the corresponding eikonal amplitudes. Since the soft function in Eq. (5)

---

[1] Soft-collinear emissions can enter in both the soft and the jet functions, so that different options exist, all aimed at avoiding double counting. In the factorization approach applied in this work, the jet functions include both, collinear non-soft and soft-collinear emissions, whereas each soft function describes only soft wide-angle gluon emissions (and absorptions) from the initial and final-state partons [22, 31, 34].

is defined as a product of two operators, it has to be renormalized multiplicatively:

$$S_{LI}^{\{f\}(B)} = \left(Z_S^{\{f\}\dagger}\right)_{LB} S_{BA}^{\{f\}} \left(Z_S^{\{f\}}\right)_{AI}, \tag{8}$$

where the superscript (B) on the left-hand side denotes the bare soft function and the Z_S matrix includes the renormalization counter-terms.

Applying the $\mu\, d/d\mu$ operation on Eq. (8) and considering that bare quantities do not depend on the renormalization scale μ, one can derive a renormalization group equation, which assumes the form [35, 36]

$$\mu\frac{d}{d\mu}S_{LI}^{\{f\}} = \left(\mu\frac{\partial}{\partial\mu} + \beta(\alpha_s)\frac{\partial}{\partial\alpha_s}\right)S_{LI}^{\{f\}} = -\left(\Gamma_S^{\{f\}}\right)_{LB}^{\dagger} S_{BI}^{\{f\}} - S_{LA}^{\{f\}}\left(\Gamma_S^{\{f\}}\right)_{AI}, \tag{9}$$

where $\beta(\alpha_s)$ is the QCD β-function. The matrices $\Gamma_S^{\{f\}}$ are process-specific functions of g through α_s. They depend on the process kinematics and color structure. They are referred to as *soft anomalous dimension matrices* in the literature. The solution of the equation above gives the resummation of all logarithms of the scale μ. By comparing Eq. (8) and Eq. (9) one arrives at the following expression for the soft anomalous dimension matrices at one-loop in the $\overline{\text{MS}}$ scheme:

$$\left(\Gamma_S^{\{f\}}\right)_{LI}(\alpha_s) = -\alpha_s\frac{\partial}{\partial\alpha_s}\text{Res}_{\epsilon\to 0}\left(Z_S^{\{f\}}\right)_{LI}(\alpha_s,\epsilon), \tag{10}$$

which indicates that soft anomalous dimensions are partial derivatives of residues of the UV poles contained in the $Z_S^{\{f\}}$ matrices. The solution of Eq. (9) can be written as

$$S(\mu) = \overline{\mathcal{P}}\exp\left[\int_{\mu_0}^{\mu}\frac{d\mu'}{\mu'}\Gamma_S^{\dagger}(\alpha_s(\mu'^2))\right]S(\mu_0)\mathcal{P}\exp\left[\int_{\mu_0}^{\mu}\frac{d\mu'}{\mu'}\Gamma_S(\alpha_s(\mu'^2))\right], \tag{11}$$

where $\mathcal{P}$ and $\overline{\mathcal{P}}$ refer to path-ordered exponentials in the same and in the opposite sense as the integration variable μ, respectively, and we have suppressed the superscripts $\{f\}$ on top of Γ_S and S to lighten the notation.

Hence, having the soft anomalous dimension matrix, enables us to determine the soft matrix, provided that this matrix is known at an initial scale μ_0. $S(\mu_0)$ can be fixed by matching the leading-order expansion of the resummed cross section to the result of a leading-order exact calculation.

The soft anomalous dimension matrices have a perturbative expansion, driven by the definition of the eikonal cross section, Eq. (5):

$$\Gamma_S = \left(\frac{\alpha_s}{2\pi}\right)\Gamma_S^{(1)} + \left(\frac{\alpha_s}{2\pi}\right)^2\Gamma_S^{(2)} + \mathcal{O}(\alpha_s^3). \tag{12}$$

The result of this expansion can be expressed diagrammatically by means of *Wilson webs* (for a review on webs see e.g. Ref. [37]), which are generated in the following way:

- all initial and final state particles are connected to the common vertex;

- the external partons, which are involved in the QCD interaction, are represented by Wilson lines;

- at one-loop level, one has to consider all possible single gluon exchanges between the Wilson legs.

The Feynman rules involving the Wilson lines are somewhat different from the standard QCD Feynman rules involving quarks and gluons and are called *eikonal Feynman rules*. In the following we adopt for them the prescriptions of Ref. [38].

3   Soft anomalous dimension matrices for $t\bar{t}j$ hadroproduction

At leading order the hadronic process $p + p \rightarrow t\bar{t} + \text{jet}$ consists of the following partonic subprocesses:

$$
\begin{aligned}
&1) \quad q + \bar{q} \rightarrow t + \bar{t} + g\,, \\
&2) \quad q + g \rightarrow t + \bar{t} + q\,, \qquad g + q \rightarrow t + \bar{t} + q\,, \\
&3) \quad \bar{q} + g \rightarrow t + \bar{t} + \bar{q}\,, \qquad g + \bar{q} \rightarrow t + \bar{t} + \bar{q}\,, \\
&4) \quad g + g \rightarrow t + \bar{t} + g\,.
\end{aligned}
\tag{13}
$$

Notice that the $t\bar{t}q$ and $t\bar{t}\bar{q}$ production processes is not symmetric with respect to the exchange of the initial state particles and hence, we have to consider both the qg and the gq channels explicitly.

From the point of view of color space, processes 2) and 3) do not differ from process 1). This is because all these three processes involve the same color vertices. Hence, we only need to work out processes 1) and 4) explicitly. Results for processes 2) and 3) can be inferred from those of process 1) by relabeling the indices. The color structure of this and other $2 \rightarrow 3$ processes has already been analyzed in Ref. [39]. For our calculations we have used the same color bases presented there and reported in Appendix A for completeness.

Let us discuss the case of the $q\bar{q} \rightarrow t\bar{t}g$ subprocess explicitly. The same principles apply to the gg induced subprocess. Figure 1 shows Wilson-web graphs corresponding to all possible one-loop soft gluon exchanges between the involved partons, plus the self-energy corrections for the heavy quark and antiquark (on the other hand, for each massless parton the self-energy contribution vanishes because of the scaleless loop integral). The corresponding amplitudes for these graphs, obtained by applying the eikonal Feynman rules in Ref. [38], are summarized in Table 1, where we factorize the kinematical (κ_{ij}) and color parts ($\mathscr{F}_{ij}$). Similarly, Table 2 reports the amplitudes for the Wilson web graphs relevant for the $gg \rightarrow t\bar{t}g$ subprocess. These graphs are analogous to those reported in Fig. 1, except for the initial-state Wilson lines (see caption of Fig. 1).

We work in a general axial gauge, introducing a vector n^{μ}, whose components act as gauge parameters, which satisfies the conditions $n \cdot A = 0$, $n^2 \neq 0$. This simplifies the
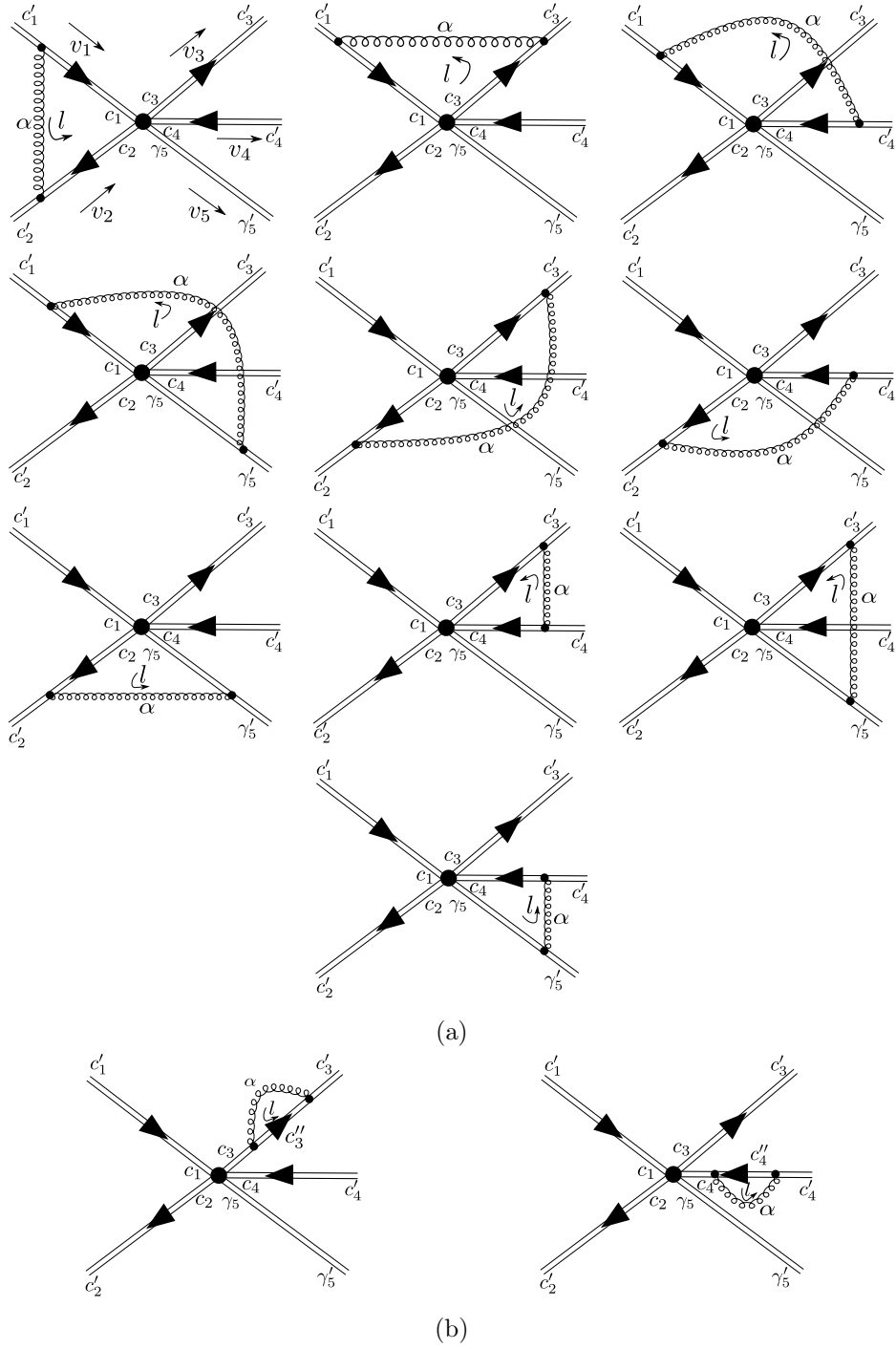
Figure 1: One-loop corrections to the soft function of the $q\bar{q} \to t\bar{t}g$ partonic subprocess: (a) vertex corrections, (b) heavy-quark self-energies. Double lines with arrow correspond to quark Wilson lines, whereas lines without arrow correspond to gluon Wilson lines. The direction of a curved arrow shows the momentum flow inside the loop. The Wilson webs for the $g\bar{g} \to t\bar{t}g$ process can be obtained by substituting the initial-state quark and antiquark Wilson lines with gluon Wilson lines and leaving all the rest the same.

8

Connection $(i-j)$	Kinematical part (κ_{ij}) before integration	Color part $(\mathscr{F}_{ij})$
$1-2$	$\dfrac{v_1^\mu}{-v_1\cdot l+i\epsilon}\dfrac{-v_2^\nu}{v_2\cdot l+i\epsilon}\dfrac{N_{\mu\nu}(l)}{l^2+i\epsilon}$	$T^\alpha_{c_1c_1'}T^\alpha_{c_2'c_2}\delta_{c_3c_3'}\delta_{c_4c_4'}\delta_{\gamma_5\gamma_5'}$
$1-3$	$\dfrac{v_1^\mu}{v_1\cdot l+i\epsilon}\dfrac{v_3^\nu}{v_3\cdot l+i\epsilon}\dfrac{N_{\mu\nu}(l)}{l^2+i\epsilon}$	$T^\alpha_{c_1c_1'}T^\alpha_{c_3'c_3}\delta_{c_2c_2'}\delta_{c_4c_4'}\delta_{\gamma_5\gamma_5'}$
$1-4$	$\dfrac{v_1^\mu}{v_1\cdot l+i\epsilon}\dfrac{-v_4^\nu}{v_4\cdot l+i\epsilon}\dfrac{N_{\mu\nu}(l)}{l^2+i\epsilon}$	$T^\alpha_{c_1c_1'}T^\alpha_{c_4c_4'}\delta_{c_2c_2'}\delta_{c_3c_3'}\delta_{\gamma_5\gamma_5'}$
$1-5$	$\dfrac{v_1^\mu}{v_1\cdot l+i\epsilon}\dfrac{-v_5^\nu}{v_5\cdot l+i\epsilon}\dfrac{N_{\mu\nu}(l)}{l^2+i\epsilon}$	$T^\alpha_{c_1c_1'}(-if^{\alpha\gamma_5\gamma_5'})\delta_{c_2c_2'}\delta_{c_3c_3'}\delta_{c_4c_4'}$
$2-3$	$\dfrac{-v_2^\mu}{-v_2\cdot l+i\epsilon}\dfrac{v_3^\nu}{-v_3\cdot l+i\epsilon}\dfrac{N_{\mu\nu}(l)}{l^2+i\epsilon}$	$T^\alpha_{c_2'c_2}T^\alpha_{c_3'c_3}\delta_{c_1c_1'}\delta_{c_4c_4'}\delta_{\gamma_5\gamma_5'}$
$2-4$	$\dfrac{-v_2^\mu}{-v_2\cdot l+i\epsilon}\dfrac{-v_4^\nu}{-v_4\cdot l+i\epsilon}\dfrac{N_{\mu\nu}(l)}{l^2+i\epsilon}$	$T^\alpha_{c_2'c_2}T^\alpha_{c_4c_4'}\delta_{c_1c_1'}\delta_{c_3c_3'}\delta_{\gamma_5\gamma_5'}$
$2-5$	$\dfrac{-v_2^\mu}{-v_2\cdot l+i\epsilon}\dfrac{v_5^\nu}{-v_5\cdot l+i\epsilon}\dfrac{N_{\mu\nu}(l)}{l^2+i\epsilon}$	$T^\alpha_{c_2'c_2}(-if^{\alpha\gamma_5'\gamma_5})\delta_{c_1c_1'}\delta_{c_3c_3'}\delta_{c_4'c_4}$
$3-4$	$\dfrac{v_3^\mu}{-v_3\cdot l+i\epsilon}\dfrac{-v_4^\nu}{v_4\cdot l+i\epsilon}\dfrac{N_{\mu\nu}(l)}{l^2+i\epsilon}$	$T^\alpha_{c_3'c_3}T^\alpha_{c_4c_4'}\delta_{c_1c_1'}\delta_{c_2c_2'}\delta_{\gamma_5\gamma_5'}$
$3-5$	$\dfrac{v_3^\mu}{-v_3\cdot l+i\epsilon}\dfrac{-v_5^\nu}{v_5\cdot l+i\epsilon}\dfrac{N_{\mu\nu}(l)}{l^2+i\epsilon}$	$T^\alpha_{c_3'c_3}(-if^{\alpha\gamma_5\gamma_5'})\delta_{c_1c_1'}\delta_{c_2c_2'}\delta_{c_4c_4'}$
$4-5$	$\dfrac{v_4^\mu}{-v_4\cdot l+i\epsilon}\dfrac{-v_5^\nu}{v_5\cdot l+i\epsilon}\dfrac{N_{\mu\nu}(l)}{l^2+i\epsilon}$	$T^\alpha_{c_4c_4'}(-if^{\alpha\gamma_5\gamma_5'})\delta_{\gamma_1\gamma_1'}\delta_{\gamma_2\gamma_2'}\delta_{c_3c_3'}$
$3-3$	$\dfrac{v_3^\mu}{v_3\cdot l+i\epsilon}\dfrac{v_3^\nu}{-v_3\cdot l+i\epsilon}\dfrac{N_{\mu\nu}(l)}{l^2+i\epsilon}$	$T^\alpha_{c_3''c_3}T^\alpha_{c_3'c_3''}\delta_{c_1c_1'}\delta_{c_2c_2'}\delta_{c_4c_4'}\delta_{\gamma_5\gamma_5'}$
$4-4$	$\dfrac{-v_4^\mu}{v_4\cdot l+i\epsilon}\dfrac{-v_4^\nu}{-v_4\cdot l+i\epsilon}\dfrac{N_{\mu\nu}(l)}{l^2+i\epsilon}$	$T^\alpha_{c_4''c_4}T^\alpha_{c_4'c_4''}\delta_{c_1c_1'}\delta_{c_2c_2'}\delta_{c_3c_3'}\delta_{\gamma_5\gamma_5'}$

Table 1: Amplitudes for the graphs shown in Fig. 1. The first column specifies the partons which exchange a soft gluon, the second and third column show the corresponding kinematic part κ_{ij} and color part $\mathscr{F}_{ij}$. For the definition of the various elements appearing in the color part see Appendix A. The first ten rows correspond to vertex corrections (Fig. 1a), whereas the last two rows correspond to the self-energy contributions (Fig. 1b).

analysis, by ensuring that collinear logarithms appear only within the jet functions [31]. In this gauge the gluon propagator entering the kinematical factors κ_{ij} is given by

$$N^{\mu\nu}(k) = g^{\mu\nu} - \frac{n^\mu k^\nu + n^\nu k^\mu}{n\cdot k} + n^2\frac{k^\mu k^\nu}{(n\cdot k)^2}\,, \tag{14}$$

where $g^{\mu\nu}$ is the metric tensor. To deal with the unphysical singularities introduced by the axial gauge we use the principal value prescription [40]:

$$\frac{\mathscr{P}}{(l\cdot n)^\beta} = \frac{1}{2}\left(\frac{1}{(l\cdot n+i\epsilon)^\beta} + (-1)^\beta\frac{1}{(-l\cdot n+i\epsilon)^\beta}\right)\,, \tag{15}$$

where β denotes a power not restricted to integer values. As a result, each integral over the kinematic part can be reduced to the following form:

$$\begin{aligned}
\omega_{ij}(\delta_i v_i, \delta_j v_j, \Delta_i, \Delta_j) &= g^2\int\frac{d^D\ell}{(2\pi)^D}\kappa_{ij}(\delta_i v_i, \delta_j v_j, \Delta_i, \Delta_j; \ell)\\
&= \Delta_i\Delta_j\delta_i\delta_j\Big(I_1(\delta_i v_i, \delta_j v_j) - \frac{1}{2}I_2(\delta_i v_i, n) - \frac{1}{2}I_2(\delta_i v_i, -n)-\\
&\qquad - \frac{1}{2}I_3(\delta_j v_j, n) - \frac{1}{2}I_3(\delta_j v_j, -n) + I_4(n^2)\Big)\,,
\end{aligned} \tag{16}$$

9

Connection $(i-j)$	Kinematical part (κ_{ij}) before integration	Color part $(\mathscr{F}_{ij})$
$1-2$	$\frac{v_1^\mu}{-v_1\cdot l+i\epsilon}\frac{-v_2^\nu}{v_2\cdot l+i\epsilon}\frac{N_{\mu\nu}(l)}{l^2+i\epsilon}$	$-f^{\alpha\gamma_1\gamma_1'}f^{\alpha\gamma_2'\gamma_2}\delta_{c_3c_3'}\delta_{c_4c_4'}\delta_{\gamma_5\gamma_5'}$
$1-3$	$\frac{-v_1^\mu}{v_1\cdot l+i\epsilon}\frac{v_3^\nu}{v_3\cdot l+i\epsilon}\frac{N_{\mu\nu}(l)}{l^2+i\epsilon}$	$(-if^{\alpha\gamma_1'\gamma_1})T^\alpha_{c_3'c_3}\delta_{\gamma_2\gamma_2'}\delta_{c_4c_4'}\delta_{\gamma_5\gamma_5'}$
$1-4$	$\frac{-v_1^\mu}{v_1\cdot l+i\epsilon}\frac{-v_4^\nu}{v_4\cdot l+i\epsilon}\frac{N_{\mu\nu}(l)}{l^2+i\epsilon}$	$(-if^{\alpha\gamma_1'\gamma_1})T^\alpha_{c_4c_4'}\delta_{\gamma_2\gamma_2'}\delta_{c_3c_3'}\delta_{\gamma_5\gamma_5'}$
$1-5$	$\frac{-v_1^\mu}{v_1\cdot l+i\epsilon}\frac{-v_5^\nu}{v_5\cdot l+i\epsilon}\frac{N_{\mu\nu}(l)}{l^2+i\epsilon}$	$-f^{\alpha\gamma_1'\gamma_1}f^{\alpha\gamma_5\gamma_5'}\delta_{\gamma_2\gamma_2'}\delta_{c_3c_3'}\delta_{c_4c_4'}$
$2-3$	$\frac{v_2^\mu}{-v_2\cdot l+i\epsilon}\frac{v_3^\nu}{-v_3\cdot l+i\epsilon}\frac{N_{\mu\nu}(l)}{l^2+i\epsilon}$	$(-if^{\alpha\gamma_2\gamma_2'})T^\alpha_{c_3'c_3}\delta_{\gamma_1\gamma_1'}\delta_{c_4c_4'}\delta_{\gamma_5\gamma_5'}$
$2-4$	$\frac{v_2^\mu}{-v_2\cdot l+i\epsilon}\frac{-v_4^\nu}{-v_4\cdot l+i\epsilon}\frac{N_{\mu\nu}(l)}{l^2+i\epsilon}$	$(-if^{\alpha\gamma_2\gamma_2'})T^\alpha_{c_4c_4'}\delta_{\gamma_1\gamma_1'}\delta_{c_3c_3'}\delta_{\gamma_5\gamma_5'}$
$2-5$	$\frac{v_2^\mu}{-v_2\cdot l+i\epsilon}\frac{v_5^\nu}{-v_5\cdot l+i\epsilon}\frac{N_{\mu\nu}(l)}{l^2+i\epsilon}$	$-f^{\alpha\gamma_2\gamma_2'}f^{\alpha\gamma_5'\gamma_5}\delta_{c_1c_1'}\delta_{c_3c_3'}\delta_{c_4'c_4}$
$3-4$	$\frac{v_3^\mu}{-v_3\cdot l+i\epsilon}\frac{-v_4^\nu}{v_4\cdot l+i\epsilon}\frac{N_{\mu\nu}(l)}{l^2+i\epsilon}$	$T^\alpha_{c_3'c_3}T^\alpha_{c_4c_4'}\delta_{\gamma_1\gamma_1'}\delta_{\gamma_2\gamma_2'}\delta_{\gamma_5\gamma_5'}$
$3-5$	$\frac{v_3^\mu}{-v_3\cdot l+i\epsilon}\frac{-v_5^\nu}{v_5\cdot l+i\epsilon}\frac{N_{\mu\nu}(l)}{l^2+i\epsilon}$	$T^\alpha_{c_3'c_3}(-if^{\alpha\gamma_5\gamma_5'})\delta_{\gamma_1\gamma_1'}\delta_{\gamma_2\gamma_2'}\delta_{c_4c_4'}$
$4-5$	$\frac{-v_4^\mu}{-v_4\cdot l+i\epsilon}\frac{-v_5^\nu}{v_5\cdot l+i\epsilon}\frac{N_{\mu\nu}(l)}{l^2+i\epsilon}$	$T^\alpha_{c_4c_4'}(-if^{\alpha\gamma_5\gamma_5'})\delta_{\gamma_1\gamma_1'}\delta_{\gamma_2\gamma_2'}\delta_{c_3c_3'}$
$3-3$	$\frac{v_3^\mu}{v_3\cdot l+i\epsilon}\frac{v_3^\nu}{-v_3\cdot l+i\epsilon}\frac{N_{\mu\nu}(l)}{l^2+i\epsilon}$	$T^\alpha_{c_3''c_3}T^\alpha_{c_3'c_3''}\delta_{\gamma_1\gamma_1'}\delta_{\gamma_2\gamma_2'}\delta_{c_4c_4'}\delta_{\gamma_5\gamma_5'}$
$4-4$	$\frac{-v_4^\mu}{v_4\cdot l+i\epsilon}\frac{-v_4^\nu}{-v_4\cdot l+i\epsilon}\frac{N_{\mu\nu}(l)}{l^2+i\epsilon}$	$T^\alpha_{c_4''c_4}T^\alpha_{c_4'c_4''}\delta_{c_1c_1'}\delta_{c_2c_2'}\delta_{c_3c_3'}\delta_{\gamma_5\gamma_5'}$

Table 2: Same as Table 1, but for the $gg \to t\bar{t}g$ subprocess.

where v_i^μ is the dimensionless velocity vector of the parton i with momentum p_i^μ, defined as:

$$v_i^\mu = \frac{p_i^\mu}{Q}\,, \tag{17}$$

with $Q = \sqrt{s/2}$, where s is the partonic center-of-mass energy. A term Δ_i is associated to each quark and antiquark, assuming values of $+1$ and -1, respectively. In case of gluons $\Delta_i = 1$ if a soft gluon line is emitted below the eikonal line and $\Delta_i = -1$ otherwise [35]. The term δ_i assumes value $+1$ or -1 depending if the direction of the momentum of the exchanged gluon is the same or opposite of the direction of momentum of line i. More details on Δ_i and δ_i, as well as on the integrals I_1, I_2, I_3 and I_4 in Eq. (16), can be found in Ref. [38].

Considering the one-loop soft-anomalous dimension expression in Eq. (10), we are only interested in the simple poles of the integrals above. The UV poles of the integrals $I_1 - I_4$ appearing in Eq. (16) are given in Ref. [38]. One can observe that plugging these integrals into Eq. (16) causes double poles to cancel. There are two sources of gauge dependence in these integrals: i) the gauge dependence coming from the vertex-correction webs, among those in Fig. 1a, where the wide-angle soft gluon is exchanged between a massive quark and another parton, is canceled by the heavy-quark self-energy contributions depicted in Fig. 1b; ii) the remaining gauge dependence originates from the massless partons and it is contained in terms of the following form

$$\nu_i = \frac{(v_i \cdot n)^2}{|n|^2}\,. \tag{18}$$

They remain present at the level of the soft function and are expected to finally cancel upon substitution of the soft function into the fully factorized expression of the partonic cross section, thanks to their combination with similar terms coming from the jet functions, as also discussed in Ref. [38].

The final result for the soft anomalous dimension matrix elements can be written as:

$$(\Gamma_S)^{AB} = \sum_{i,j=1;i\leq j}^{5} \mathcal{F}_{ij}^{AB}\Omega_{ij}\,, \tag{19}$$

where the sum runs over all diagrams of Fig. 1, $\mathcal{F}_{ij}$ are color matrices, corresponding to Wilson webs with soft gluon exchange between partons i and j, A and B are indices running over the elements of the color basis and $\Omega_{ij} = (\omega_{ij})_{\text{UV divergent}}$ corresponds to the sum of simple poles of ω_{ij} (see Eq. (16)), extracted using the technique described above.

In Eq. (19) the self-energy contributions of Fig. 1b enter with a prefactor $\frac{1}{2}$, due to the way the quark (antiquark) wave-function renormalization is performed:

$$\psi^{(B)} = Z_\psi^{1/2}\psi\,. \tag{20}$$

Concerning the color decomposition of the amplitude associated to each Wilson web in the color basis, in simple cases, as the one discussed in Appendix B, one is able to manipulate the color tensor structure and visually recognize linear combinations in terms of the elements of the color basis, which allow for a manual reconstruction of $\mathcal{F}_{ij}$. However, for more complicated cases, like those for the $gg \to t\bar{t}g$ subprocess, requiring a color basis with many elements, it becomes hard to express the color structure in terms of the basis tensors in a straightforward way. Hence, we have developed a more general and automatized approach to achieve this task. Let us define the following tensor:

$$G_{AB} = \text{tr}\left(\mathbf{c}_A \mathbf{c}'_B{}^\dagger \sum_{i,j;i\leq j} \Omega_{ij}\mathscr{F}_{ij}\right), \tag{21}$$

where $\{\mathbf{c}\}$ is the color basis for the process before soft wide-angle gluon exchange, $\{\mathbf{c}'\}$ is the color basis in terms of color indices after soft wide-angle gluon exchange, the $\mathscr{F}_{ij}$ terms are taken directly from the Wilson web graphs and collected in Table 1 and 2, and the trace is performed over color space. The idea of this procedure is to contract the open color indices and algebraically manipulate the resulting terms which are scalars in color space. This way we perform the color decomposition of the amplitude of each Wilson web. Then, the components of the soft anomalous dimension can be extracted according to

$$\Gamma_{IJ} = \left(S^{(0)}\right)^{-1}_{IK} G_{KJ}\,. \tag{22}$$

These operations can be implemented using computer algebra systems, which makes it possible to perform the calculations even for complicated processes.

4 Results for one-loop soft anomalous dimension matrices

Following the strategy outlined in Section 3 and using the computer algebra system `FORM` [41], the package `FORMSoft` [42] has been developed to perform analytical calculations of soft anomalous dimension matrices at one loop. Starting from color bases hard-coded by the user, the rest is done automatically. The generation of Wilson webs and of their amplitudes, which are input for `FORMSoft`, has been performed automatically as well, using the `C`-program `WilsonWebs` [43], which supports planar Wilson web generation up to six loops. In the following we present explicitly the analytical results of the calculation for the $q\bar{q}$- and gg-induced subprocesses.

4.1 $q\bar{q}$ channel

The Born-level soft matrix calculated according to Eq. (7) is given by

$$S^{(0)} = \begin{pmatrix} \frac{N_c(N_c^2-1)}{2} & 0 & 0 & 0 \\ 0 & \frac{N_c(N_c^2-1)}{2} & 0 & 0 \\ 0 & 0 & \frac{N_c(N_c^2-1)}{4} & 0 \\ 0 & 0 & 0 & \frac{(N_c^2-1)(N_c^2-4)}{4N_c} \end{pmatrix}. \tag{23}$$

We explicitly verified that $S^{(0)}$ satisfies the consistency check

$$tr(H_{AB}^{(0)}S_{BC}^{(0)}) = |\mathcal{M}|^2\,, \tag{24}$$

where $H^{(0)}$ is the color decomposed Born-level hard-scattering matrix entering the refactorization formula for the partonic cross section and $|\mathcal{M}|^2$ is the squared amplitude of the partonic process at leading order. Performing the calculation of the color part of the soft anomalous dimension matrix at one-loop, we are able to reproduce the results published in [39], confirming their correctness, using their same color basis, also reported in Appendix A.1 for completeness. After including the kinematical factors as well, we get the following results for the elements of the one-loop Γ matrix, considering the perturbative expansion in Eq. (12):

$$\Gamma_{1,1}^{(1)} = \frac{1}{2N_c}\left[2L_\beta + N_c^2\left(-2\log\left(\nu_5\right) + 2\log\left(v_{35}\right) + 2\log\left(v_{45}\right) + 2\log\left(\frac{s}{m_t^2}\right) - \log\left(16\right) + 2\right)\right.$$

$$\left. + \left(N_c^2 - 1\right)\left(-\log\left(\nu_1\right) - \log\left(\nu_2\right) + 2i\pi\right) + \log\left(4\right)\right]$$

$$\Gamma_{1,2}^{(1)} = \frac{1}{N_c}\left[\log\left(v_{13}\right) - \log\left(v_{14}\right) - \log\left(v_{23}\right) + \log\left(v_{24}\right)\right]$$

$$\Gamma_{1,3}^{(1)} = -\frac{\log\left(v_{13}\right)}{2} - \frac{\log\left(v_{14}\right)}{2} + \log\left(v_{15}\right) + \frac{\log\left(v_{23}\right)}{2} + \frac{\log\left(v_{24}\right)}{2} - \log\left(v_{25}\right)$$

$$\Gamma_{1,4}^{(1)} = \frac{N_c^2 - 4}{2N_c^2}\left[\log\left(v_{13}\right) - \log\left(v_{14}\right) - \log\left(v_{23}\right) + \log\left(v_{24}\right)\right]$$

$$\Gamma_{2,1}^{(1)} = \frac{1}{N_c} \left[\log\left(v_{13}\right) - \log\left(v_{14}\right) - \log\left(v_{23}\right) + \log\left(v_{24}\right) \right]$$

$$\Gamma_{2,2}^{(1)} = \frac{1}{2N_c} \left[N_c^2 \left(-2\log\left(\nu_5\right) + 2\log\left(v_{15}\right) + 2\log\left(v_{25}\right) - \log\left(16\right) + 2\right) + \left(N_c^2 - 1\right)\left(-2L_\beta - \log\left(\nu_1\right)\right.\right.$$
$$\left.\left. - \log\left(\nu_2\right)\right) + \log\left(4\right) - 2i\pi \right]$$

$$\Gamma_{2,3}^{(1)} = -\frac{\log\left(v_{13}\right)}{2} + \frac{\log\left(v_{14}\right)}{2} - \frac{\log\left(v_{23}\right)}{2} + \frac{\log\left(v_{24}\right)}{2} + \log\left(v_{35}\right) - \log\left(v_{45}\right)$$

$$\Gamma_{2,4}^{(1)} = \frac{N_c^2 - 4}{2N_c^2} \left[\log\left(v_{13}\right) - \log\left(v_{14}\right) - \log\left(v_{23}\right) + \log\left(v_{24}\right) \right]$$

$$\Gamma_{3,1}^{(1)} = -\log\left(v_{13}\right) - \log\left(v_{14}\right) + 2\log\left(v_{15}\right) + \log\left(v_{23}\right) + \log\left(v_{24}\right) - 2\log\left(v_{25}\right)$$

$$\Gamma_{3,2}^{(1)} = -\log\left(v_{13}\right) + \log\left(v_{14}\right) - \log\left(v_{23}\right) + \log\left(v_{24}\right) + 2\log\left(v_{35}\right) - 2\log\left(v_{45}\right)$$

$$\Gamma_{3,3}^{(1)} = \frac{1}{2N_c} \left[2L_\beta + N_c^2 \left(-2\log\left(\nu_5\right) + \log\left(v_{15}\right) + \log\left(v_{25}\right) + \log\left(v_{35}\right) + \log\left(v_{45}\right) + 2\log\left(\frac{s}{m_t^2}\right)\right.\right.$$
$$\left.\left. - \log\left(16\right) + 2\right) + \left(N_c^2 - 2\right)\left(\log\left(v_{13}\right) + \log\left(v_{24}\right)\right) + \left(N_c^2 - 1\right)\left(-\log\left(\nu_1\right) - \log\left(\nu_2\right)\right)\right.$$
$$\left. + 2\log\left(v_{14}\right) + 2\log\left(v_{23}\right) + \log\left(4\right) - 2i\pi \right]$$

$$\Gamma_{3,4}^{(1)} = \frac{N_c^2 - 4}{2N_c} \left[-\log\left(v_{13}\right) + \log\left(v_{15}\right) + \log\left(v_{24}\right) - \log\left(v_{25}\right) + \log\left(v_{35}\right) - \log\left(v_{45}\right) \right]$$

$$\Gamma_{4,1}^{(1)} = \log\left(v_{13}\right) - \log\left(v_{14}\right) - \log\left(v_{23}\right) + \log\left(v_{24}\right)$$

$$\Gamma_{4,2}^{(1)} = \log\left(v_{13}\right) - \log\left(v_{14}\right) - \log\left(v_{23}\right) + \log\left(v_{24}\right)$$

$$\Gamma_{4,3}^{(1)} = \frac{N_c}{2} \left[-\log\left(v_{13}\right) + \log\left(v_{15}\right) + \log\left(v_{24}\right) - \log\left(v_{25}\right) + \log\left(v_{35}\right) - \log\left(v_{45}\right) \right]$$

$$\Gamma_{4,4}^{(1)} = \frac{1}{2N_c} \left[2L_\beta + N_c^2 \left(-2\log\left(\nu_5\right) + \log\left(v_{15}\right) + \log\left(v_{25}\right) + \log\left(v_{35}\right) + \log\left(v_{45}\right) + 2\log\left(\frac{s}{m_t^2}\right)\right.\right.$$
$$\left.\left. - \log\left(16\right) + 2\right) + \left(N_c^2 - 6\right)\left(\log\left(v_{13}\right) + \log\left(v_{24}\right)\right) + \left(N_c^2 - 1\right)\left(-\log\left(\nu_1\right) - \log\left(\nu_2\right)\right)\right.$$
$$\left. + 6\log\left(v_{14}\right) + 6\log\left(v_{23}\right) + \log\left(4\right) - 2i\pi \right]$$

In the previous formula, L_β is the velocity-dependent eikonal function:

$$L_\beta = \frac{1 - 2m_t^2/s}{\beta} \left(\ln\frac{1-\beta}{1+\beta} + \pi i \right), \tag{25}$$

with $\beta = \sqrt{1 - 4m_t^2/s}$, m_t the top-quark mass and $v_{ij} = v_i v_j$, see Eq. (17). Those cases

13

where $\Gamma^{AB} \neq \Gamma^{BA}$ are related to the fact that the corresponding color components $\mathcal{F}_{ij}^{AB} \neq \mathcal{F}_{ij}^{BA}$, i.e. the $\mathcal{F}_{ij}$ matrix is in general non-symmetric.

4.2 gg channel

The results of our calculation of the Born-level soft matrix and one-loop color factors, using the color basis taken from Ref. [39] and reported in Appendix A.2 for completeness, with basis elements ordered as listed, are in agreement with those published in Ref. [39], confirming the correctness of the latter. For explicit expressions, we address the interested reader to that reference. On the other hand, the complete result that we obtained for the one-loop components of the soft anomalous dimension matrix including both the color and the kinematic factors, reads as follows:

$$\Gamma_{1,1}^{(1)} = \frac{1}{N_c}\left[L_\beta + N_c^2\left(-\log\left(\nu_1\right) - \log\left(\nu_2\right) - \log\left(\nu_5\right) + \log\left(v_{35}\right) + \log\left(v_{45}\right) + \log\left(\frac{s}{m_t^2}\right) - \log\left(8\right)\right.\right.$$

$$\left.\left. + 2 + 2i\pi\right) + 1\right]$$

$$\Gamma_{1,2}^{(1)} = \frac{2N_c}{N_c^2 - 1}\left[\log\left(v_{13}\right) - \log\left(v_{14}\right) - \log\left(v_{23}\right) + \log\left(v_{24}\right)\right]$$

$$\Gamma_{1,3}^{(1)} = 0$$

$$\Gamma_{1,4}^{(1)} = \frac{N_c^2}{N_c^2 - 1}\left[-\log\left(v_{13}\right) - \log\left(v_{14}\right) + 2\log\left(v_{15}\right) + \log\left(v_{23}\right) + \log\left(v_{24}\right) - 2\log\left(v_{25}\right)\right]$$

$$\Gamma_{1,5}^{(1)} = 0$$

$$\Gamma_{1,6}^{(1)} = \frac{N_c^2 - 4}{N_c^2 - 1}\left[\log\left(v_{13}\right) - \log\left(v_{14}\right) - \log\left(v_{23}\right) + \log\left(v_{24}\right)\right]$$

$$\Gamma_{1,7}^{(1)} = 0$$

$$\Gamma_{1,8}^{(1)} = 0$$

$$\Gamma_{1,9}^{(1)} = 0$$

$$\Gamma_{1,10}^{(1)} = 0$$

$$\Gamma_{1,11}^{(1)} = 0$$

$$\Gamma_{2,1}^{(1)} = \frac{1}{N_c}\left[\log\left(v_{13}\right) - \log\left(v_{14}\right) - \log\left(v_{23}\right) + \log\left(v_{24}\right)\right]$$

$$\Gamma_{2,2}^{(1)} = \frac{1}{N_c}\left[-L_\beta\left(N_c^2-1\right) + N_c^2\left(-\log\left(\nu_1\right) - \log\left(\nu_2\right) - \log\left(\nu_5\right) + \log\left(v_{15}\right) + \log\left(v_{25}\right) - \log\left(8\right)\right.\right.$$
$$\left.\left. + 2 + i\pi\right) + 1\right]$$

$$\Gamma_{2,3}^{(1)} = 0$$

$$\Gamma_{2,4}^{(1)} = -\frac{\log\left(v_{13}\right)}{2} + \frac{\log\left(v_{14}\right)}{2} - \frac{\log\left(v_{23}\right)}{2} + \frac{\log\left(v_{24}\right)}{2} + \log\left(v_{35}\right) - \log\left(v_{45}\right)$$

$$\Gamma_{2,5}^{(1)} = 0$$

$$\Gamma_{2,6}^{(1)} = 0$$

$$\Gamma_{2,7}^{(1)} = \frac{N_c^2 - 4}{2N_c^2}\left[\log\left(v_{13}\right) - \log\left(v_{14}\right) - \log\left(v_{23}\right) + \log\left(v_{24}\right)\right]$$

$$\Gamma_{2,8}^{(1)} = 0$$

$$\Gamma_{2,9}^{(1)} = 0$$

$$\Gamma_{2,10}^{(1)} = \frac{N_c + 3}{4N_c + 4}\left[\log\left(v_{13}\right) - \log\left(v_{14}\right) - \log\left(v_{23}\right) + \log\left(v_{24}\right)\right]$$

$$\Gamma_{2,11}^{(1)} = \frac{N_c - 3}{4N_c - 4}\left[\log\left(v_{13}\right) - \log\left(v_{14}\right) - \log\left(v_{23}\right) + \log\left(v_{24}\right)\right]$$

$$\Gamma_{3,1}^{(1)} = 0$$

$$\Gamma_{3,2}^{(1)} = 0$$

$$\Gamma_{3,3}^{(1)} = \frac{1}{N_c}\left[-L_\beta\left(N_c^2-1\right) + N_c^2\left(-\log\left(\nu_1\right) - \log\left(\nu_2\right) - \log\left(\nu_5\right) + \log\left(v_{15}\right) + \log\left(v_{25}\right) - \log\left(8\right)\right.\right.$$
$$\left.\left. + 2 + i\pi\right) + 1\right]$$

$$\Gamma_{3,4}^{(1)} = 0$$

$$\Gamma_{3,5}^{(1)} = -\frac{\log\left(v_{13}\right)}{2} + \frac{\log\left(v_{14}\right)}{2} - \frac{\log\left(v_{23}\right)}{2} + \frac{\log\left(v_{24}\right)}{2} + \log\left(v_{35}\right) - \log\left(v_{45}\right)$$

$$\Gamma_{3,6}^{(1)} = \frac{\log\left(v_{13}\right)}{2} - \frac{\log\left(v_{14}\right)}{2} - \frac{\log\left(v_{23}\right)}{2} + \frac{\log\left(v_{24}\right)}{2}$$

$$\Gamma_{3,7}^{(1)} = 0$$

$$\Gamma_{3,8}^{(1)} = 0$$

$$\Gamma_{3,9}^{(1)} = \frac{\log\left(v_{13}\right)}{2} - \frac{\log\left(v_{14}\right)}{2} - \frac{\log\left(v_{23}\right)}{2} + \frac{\log\left(v_{24}\right)}{2}$$

$$\Gamma_{3,10}^{(1)} = 0$$

$$\Gamma_{3,11}^{(1)} = 0$$

$$\Gamma_{4,1}^{(1)} = -\log(v_{13}) - \log(v_{14}) + 2\log(v_{15}) + \log(v_{23}) + \log(v_{24}) - 2\log(v_{25})$$

$$\Gamma_{4,2}^{(1)} = -\log(v_{13}) + \log(v_{14}) - \log(v_{23}) + \log(v_{24}) + 2\log(v_{35}) - 2\log(v_{45})$$

$$\Gamma_{4,3}^{(1)} = 0$$

$$\Gamma_{4,4}^{(1)} = \frac{1}{N_c}\left[L_\beta + N_c^2\left(-\log(\nu_1) - \log(\nu_2) - \log(\nu_5) + \frac{\log(v_{13})}{4} + \frac{\log(v_{14})}{4} + \frac{\log(v_{15})}{2} + \frac{\log(v_{23})}{4} \right.\right.$$
$$\left.\left. + \frac{\log(v_{24})}{4} + \frac{\log(v_{25})}{2} + \frac{\log(v_{35})}{2} + \frac{\log(v_{45})}{2} + \log\left(\frac{s}{m_t^2}\right) - \frac{\log(4096)}{4} + 2 + i\pi \right) + 1 \right]$$

$$\Gamma_{4,5}^{(1)} = \frac{N_c^2 - 4}{4N_c}[\log(v_{13}) - \log(v_{14}) - \log(v_{23}) + \log(v_{24})]$$

$$\Gamma_{4,6}^{(1)} = \frac{N_c^2 - 4}{4N_c}[-\log(v_{13}) + \log(v_{14}) - \log(v_{23}) + \log(v_{24}) + 2\log(v_{35}) - 2\log(v_{45})]$$

$$\Gamma_{4,7}^{(1)} = \frac{N_c^2 - 4}{4N_c}[-\log(v_{13}) - \log(v_{14}) + 2\log(v_{15}) + \log(v_{23}) + \log(v_{24}) - 2\log(v_{25})]$$

$$\Gamma_{4,8}^{(1)} = 0$$

$$\Gamma_{4,9}^{(1)} = 0$$

$$\Gamma_{4,10}^{(1)} = \frac{N_c + 3}{4N_c + 4}[\log(v_{13}) + \log(v_{14}) - 2\log(v_{15}) - \log(v_{23}) - \log(v_{24}) + 2\log(v_{25})]$$

$$\Gamma_{4,11}^{(1)} = \frac{N_c - 3}{4N_c - 4}[-\log(v_{13}) - \log(v_{14}) + 2\log(v_{15}) + \log(v_{23}) + \log(v_{24}) - 2\log(v_{25})]$$

$$\Gamma_{5,1}^{(1)} = 0$$

$$\Gamma_{5,2}^{(1)} = 0$$

$$\Gamma_{5,3}^{(1)} = -\log(v_{13}) + \log(v_{14}) - \log(v_{23}) + \log(v_{24}) + 2\log(v_{35}) - 2\log(v_{45})$$

$$\Gamma_{5,4}^{(1)} = \frac{N_c}{4}[\log(v_{13}) - \log(v_{14}) - \log(v_{23}) + \log(v_{24})]$$

$$\Gamma_{5,5}^{(1)} = \frac{1}{N_c}\left[L_\beta + N_c^2\left(-\log(\nu_1) - \log(\nu_2) - \log(\nu_5) + \frac{\log(v_{13})}{4} + \frac{\log(v_{14})}{4} + \frac{\log(v_{15})}{2} + \frac{\log(v_{23})}{4} \right.\right.$$
$$\left.\left. + \frac{\log(v_{24})}{4} + \frac{\log(v_{25})}{2} + \frac{\log(v_{35})}{2} + \frac{\log(v_{45})}{2} + \log\left(\frac{s}{m_t^2}\right) - \frac{\log(4096)}{4} + 2 + i\pi \right) + 1 \right]$$

$$\Gamma_{5,6}^{(1)} = \frac{N_c}{4}[-\log(v_{13}) - \log(v_{14}) + 2\log(v_{15}) + \log(v_{23}) + \log(v_{24}) - 2\log(v_{25})]$$

$$\Gamma_{5,7}^{(1)} = \frac{N_c^2 - 4}{4N_c}[-\log(v_{13}) + \log(v_{14}) - \log(v_{23}) + \log(v_{24}) + 2\log(v_{35}) - 2\log(v_{45})]$$

$$\Gamma^{(1)}_{5,8} = \frac{\log{(v_{13})}}{2} - \frac{\log{(v_{14})}}{2} - \frac{\log{(v_{23})}}{2} + \frac{\log{(v_{24})}}{2}$$

$$\Gamma^{(1)}_{5,9} = 0$$

$$\Gamma^{(1)}_{5,10} = 0$$

$$\Gamma^{(1)}_{5,11} = 0$$

$$\Gamma^{(1)}_{6,1} = \log{(v_{13})} - \log{(v_{14})} - \log{(v_{23})} + \log{(v_{24})}$$

$$\Gamma^{(1)}_{6,2} = 0$$

$$\Gamma^{(1)}_{6,3} = \log{(v_{13})} - \log{(v_{14})} - \log{(v_{23})} + \log{(v_{24})}$$

$$\Gamma^{(1)}_{6,4} = \frac{N_c}{4}[-\log{(v_{13})} + \log{(v_{14})} - \log{(v_{23})} + \log{(v_{24})} + 2\log{(v_{35})} - 2\log{(v_{45})}]$$

$$\Gamma^{(1)}_{6,5} = \frac{N_c}{4}[-\log{(v_{13})} - \log{(v_{14})} + 2\log{(v_{15})} + \log{(v_{23})} + \log{(v_{24})} - 2\log{(v_{25})}]$$

$$\Gamma^{(1)}_{6,6} = \frac{1}{N_c}\left[L_\beta + N_c^2\left(-\log{(\nu_1)} - \log{(\nu_2)} - \log{(\nu_5)} + \frac{\log{(v_{13})}}{4} + \frac{\log{(v_{14})}}{4} + \frac{\log{(v_{15})}}{2} + \frac{\log{(v_{23})}}{4}\right.\right.$$

$$\left.\left. + \frac{\log{(v_{24})}}{4} + \frac{\log{(v_{25})}}{2} + \frac{\log{(v_{35})}}{2} + \frac{\log{(v_{45})}}{2} + \log{\left(\frac{s}{m_t^2}\right)} - \frac{\log{(4096)}}{4} + 2 + i\pi\right) + 1\right]$$

$$\Gamma^{(1)}_{6,7} = \frac{N_c^2 - 12}{4N_c}[\log{(v_{13})} - \log{(v_{14})} - \log{(v_{23})} + \log{(v_{24})}]$$

$$\Gamma^{(1)}_{6,8} = 0$$

$$\Gamma^{(1)}_{6,9} = 0$$

$$\Gamma^{(1)}_{6,10} = \frac{N_c(N_c + 3)}{4N_c^2 + 12N_c + 8}[\log{(v_{13})} - \log{(v_{14})} - \log{(v_{23})} + \log{(v_{24})}]$$

$$\Gamma^{(1)}_{6,11} = \frac{N_c(N_c - 3)}{4N_c^2 - 12N_c + 8}[-\log{(v_{13})} + \log{(v_{14})} + \log{(v_{23})} - \log{(v_{24})}]$$

$$\Gamma^{(1)}_{7,1} = 0$$

$$\Gamma^{(1)}_{7,2} = \frac{N_c^2}{N_c^2 - 4}[\log{(v_{13})} - \log{(v_{14})} - \log{(v_{23})} + \log{(v_{24})}]$$

$$\Gamma^{(1)}_{7,3} = 0$$

$$\Gamma^{(1)}_{7,4} = \frac{N_c^3}{4N_c^2 - 16}[-\log{(v_{13})} - \log{(v_{14})} + 2\log{(v_{15})} + \log{(v_{23})} + \log{(v_{24})} - 2\log{(v_{25})}]$$

$$\Gamma^{(1)}_{7,5} = \frac{N_c}{4}[-\log{(v_{13})} + \log{(v_{14})} - \log{(v_{23})} + \log{(v_{24})} + 2\log{(v_{35})} - 2\log{(v_{45})}]$$

$$\Gamma_{7,6}^{(1)} = \frac{N_c(N_c^2 - 12)}{4N_c^2 - 16}[\log(v_{13}) - \log(v_{14}) - \log(v_{23}) + \log(v_{24})]$$

$$\Gamma_{7,7}^{(1)} = \frac{1}{N_c}\left[L_\beta + N_c^2\left(-\log(\nu_1) - \log(\nu_2) - \log(\nu_5) + \frac{\log(v_{13})}{4} + \frac{\log(v_{14})}{4} + \frac{\log(v_{15})}{2} + \frac{\log(v_{23})}{4}\right.\right.$$

$$\left.\left. + \frac{\log(v_{24})}{4} + \frac{\log(v_{25})}{2} + \frac{\log(v_{35})}{2} + \frac{\log(v_{45})}{2} + \log\left(\frac{s}{m_t^2}\right) - \frac{\log(4096)}{4} + 2 + i\pi\right) + 1\right]$$

$$\Gamma_{7,8}^{(1)} = \frac{N_c^2}{2N_c^2 - 8}[\log(v_{13}) + \log(v_{14}) - 2\log(v_{15}) - \log(v_{23}) - \log(v_{24}) + 2\log(v_{25})]$$

$$\Gamma_{7,9}^{(1)} = \frac{N_c}{N_c^2 - 4}[-\log(v_{13}) + \log(v_{14}) + \log(v_{23}) - \log(v_{24})]$$

$$\Gamma_{7,10}^{(1)} = 0$$

$$\Gamma_{7,11}^{(1)} = 0$$

$$\Gamma_{8,1}^{(1)} = 0$$

$$\Gamma_{8,2}^{(1)} = 0$$

$$\Gamma_{8,3}^{(1)} = 0$$

$$\Gamma_{8,4}^{(1)} = 0$$

$$\Gamma_{8,5}^{(1)} = \log(v_{13}) - \log(v_{14}) - \log(v_{23}) + \log(v_{24})$$

$$\Gamma_{8,6}^{(1)} = 0$$

$$\Gamma_{8,7}^{(1)} = \log(v_{13}) + \log(v_{14}) - 2\log(v_{15}) - \log(v_{23}) - \log(v_{24}) + 2\log(v_{25})$$

$$\Gamma_{8,8}^{(1)} = \frac{1}{N_c}\left[L_\beta + N_c^2\left(-\log(\nu_1) - \log(\nu_2) - \log(\nu_5) + \frac{\log(v_{13})}{2} + \frac{\log(v_{14})}{2} + \log(v_{15}) + \frac{\log(v_{23})}{2}\right.\right.$$

$$\left.\left. + \frac{\log(v_{24})}{2} + \log(v_{25}) + \log\left(\frac{s}{m_t^2}\right) - \frac{\log(64)}{2} + 2\right) + 1\right]$$

$$\Gamma_{8,9}^{(1)} = -\frac{\log(v_{13})}{2} + \frac{\log(v_{14})}{2} - \frac{\log(v_{23})}{2} + \frac{\log(v_{24})}{2} + \log(v_{35}) - \log(v_{45})$$

$$\Gamma_{8,10}^{(1)} = \frac{N_c(N_c + 3)}{4N_c + 8}[-\log(v_{13}) - \log(v_{14}) + 2\log(v_{15}) + \log(v_{23}) + \log(v_{24}) - 2\log(v_{25})]$$

$$\Gamma_{8,11}^{(1)} = \frac{N_c(N_c - 3)}{4N_c - 8}[\log(v_{13}) + \log(v_{14}) - 2\log(v_{15}) - \log(v_{23}) - \log(v_{24}) + 2\log(v_{25})]$$

$$\Gamma_{9,1}^{(1)} = 0$$

$$\Gamma_{9,2}^{(1)} = 0$$

$$\Gamma_{9,3}^{(1)} = 2\log(v_{13}) - 2\log(v_{14}) - 2\log(v_{23}) + 2\log(v_{24})$$

$$\Gamma_{9,4}^{(1)} = 0$$

$$\Gamma_{9,5}^{(1)} = 0$$

$$\Gamma_{9,6}^{(1)} = 0$$

$$\Gamma_{9,7}^{(1)} = \frac{1}{N_c}\left[-2\log(v_{13}) + 2\log(v_{14}) + 2\log(v_{23}) - 2\log(v_{24})\right]$$

$$\Gamma_{9,8}^{(1)} = -\frac{\log(v_{13})}{2} + \frac{\log(v_{14})}{2} - \frac{\log(v_{23})}{2} + \frac{\log(v_{24})}{2} + \log(v_{35}) - \log(v_{45})$$

$$\Gamma_{9,9}^{(1)} = \frac{1}{N_c}\left[L_\beta + N_c^2\left(-\log(\nu_1) - \log(\nu_2) - \log(\nu_5) + \frac{\log(v_{13})}{2} + \frac{\log(v_{14})}{2} + \log(v_{15}) + \frac{\log(v_{23})}{2}\right.\right.$$
$$\left.\left. + \frac{\log(v_{24})}{2} + \log(v_{25}) + \log\left(\frac{s}{m_t^2}\right) - \frac{\log(64)}{2} + 2\right) + 1\right]$$

$$\Gamma_{9,10}^{(1)} = \frac{N_c(N_c + 3)}{4N_c + 8}\left[-\log(v_{13}) + \log(v_{14}) + \log(v_{23}) - \log(v_{24})\right]$$

$$\Gamma_{9,11}^{(1)} = \frac{N_c(N_c - 3)}{4N_c - 8}\left[-\log(v_{13}) + \log(v_{14}) + \log(v_{23}) - \log(v_{24})\right]$$

$$\Gamma_{10,1}^{(1)} = 0$$

$$\Gamma_{10,2}^{(1)} = 2\log(v_{13}) - 2\log(v_{14}) - 2\log(v_{23}) + 2\log(v_{24})$$

$$\Gamma_{10,3}^{(1)} = 0$$

$$\Gamma_{10,4}^{(1)} = \log(v_{13}) + \log(v_{14}) - 2\log(v_{15}) - \log(v_{23}) - \log(v_{24}) + 2\log(v_{25})$$

$$\Gamma_{10,5}^{(1)} = 0$$

$$\Gamma_{10,6}^{(1)} = \frac{N_c - 2}{N_c}\left[\log(v_{13}) - \log(v_{14}) - \log(v_{23}) + \log(v_{24})\right]$$

$$\Gamma_{10,7}^{(1)} = 0$$

$$\Gamma_{10,8}^{(1)} = \frac{-N_c(N_c - 1) + 2}{2N_c}\left[\log(v_{13}) + \log(v_{14}) - 2\log(v_{15}) - \log(v_{23}) - \log(v_{24}) + 2\log(v_{25})\right]$$

$$\Gamma_{10,9}^{(1)} = \frac{-N_c(N_c - 1) + 2}{2N_c}\left[\log(v_{13}) - \log(v_{14}) - \log(v_{23}) + \log(v_{24})\right]$$

$$\Gamma^{(1)}_{10,10} = \frac{1}{N_c}\left[L_\beta + N_c\left(N_c\left(-\log(\nu_1) - \log(\nu_2) - \log(\nu_5) + \log\left(\frac{s}{m_t^2}\right) - \frac{\log(64)}{2} + 2 \right) + (N_c \right.\right.$$

$$\left. + 1)\left(\frac{\log(v_{13})}{2} + \frac{\log(v_{14})}{2} + \log(v_{15}) + \frac{\log(v_{23})}{2} + \frac{\log(v_{24})}{2} + \log(v_{25}) \right) - \log(v_{35})$$

$$\left.\left. - \log(v_{45}) - 2i\pi \right) + 1 \right]$$

$$\Gamma^{(1)}_{10,11} = 0$$

$$\Gamma^{(1)}_{11,1} = 0$$

$$\Gamma^{(1)}_{11,2} = 2\log(v_{13}) - 2\log(v_{14}) - 2\log(v_{23}) + 2\log(v_{24})$$

$$\Gamma^{(1)}_{11,3} = 0$$

$$\Gamma^{(1)}_{11,4} = -\log(v_{13}) - \log(v_{14}) + 2\log(v_{15}) + \log(v_{23}) + \log(v_{24}) - 2\log(v_{25})$$

$$\Gamma^{(1)}_{11,5} = 0$$

$$\Gamma^{(1)}_{11,6} = \frac{N_c + 2}{N_c}[-\log(v_{13}) + \log(v_{14}) + \log(v_{23}) - \log(v_{24})]$$

$$\Gamma^{(1)}_{11,7} = 0$$

$$\Gamma^{(1)}_{11,8} = \frac{N_c(N_c+1) - 2}{2N_c}[\log(v_{13}) + \log(v_{14}) - 2\log(v_{15}) - \log(v_{23}) - \log(v_{24}) + 2\log(v_{25})]$$

$$\Gamma^{(1)}_{11,9} = \frac{N_c(N_c+1) - 2}{2N_c}[-\log(v_{13}) + \log(v_{14}) + \log(v_{23}) - \log(v_{24})]$$

$$\Gamma^{(1)}_{11,10} = 0$$

$$\Gamma^{(1)}_{11,11} = \frac{1}{N_c}\left[L_\beta + N_c\left(N_c\left(-\log(\nu_1) - \log(\nu_2) - \log(\nu_5) + \log\left(\frac{s}{m_t^2}\right) - \frac{\log(64)}{2} + 2 \right) + (N_c \right.\right.$$

$$\left. - 1)\left(\frac{\log(v_{13})}{2} + \frac{\log(v_{14})}{2} + \log(v_{15}) + \frac{\log(v_{23})}{2} + \frac{\log(v_{24})}{2} + \log(v_{25}) \right) + \log(v_{35})$$

$$\left.\left. + \log(v_{45}) + 2i\pi \right) + 1 \right]$$

Notice that all (A, B) combinations for which $\Gamma^{AB} = 0$ are characterized by $\mathcal{F}^{AB}_{ij} = 0$ for all (i,j) pairs. Also notice that, whenever $\Gamma^{AB} = 0$, even $\Gamma^{BA} = 0$, because the zero terms are disposed symmetrically in the non-symmetric matrix $\mathcal{F}_{ij}$, i.e., if $\mathcal{F}^{AB}_{ij} = 0$, even $\mathcal{F}^{BA}_{ij} = 0$.

4.3 Discussion in the light of existing literature

We note that results of soft anomalous dimension calculation for $t\bar{t}j$ hadroproduction have been previously published in Ref. [44], working with different color bases. Different choices of color bases lead to different normalizations of the leading-order soft function matrix used in the calculation of the soft anomalous dimension matrix according to Eq. (22). Hence, an additional transformation must be applied to the results presented in this work to be able to compare them with those of Ref. [44]. Additionally, while our results refer to the general axial gauge ($n \cdot A = 0$), those of Ref. [44] are obtained in a specific axial gauge (Weyl gauge, corresponding to $A_0 = 0$). Accounting for these aspects in the comparison allows to identify some differences with the published results of Ref. [44]. In particular, in both the $gg \to t\bar{t}g$ and $q\bar{q} \to t\bar{t}g$ anomalous dimension matrices some of the elements of the soft anomalous dimension matrices turned out to be mixed up, i.e., they do not correspond to the chosen color basis. Additionally, for massless partons Ref. [44] uses the following substitution $\nu_i = \frac{1}{2}$ for the gauge-dependent terms, which is only true in the Weyl gauge in the center–of–mass frame of a $2 \to 2$ process. As a consequence of these issues, the soft anomalous dimension matrices presented in Ref. [44] are not correct. On the other hand, the results reported in Subsections 4.1 and 4.2 satisfy the consistency checks discussed in the following, besides the check in Eq. (24).

5 Probing the infrared poles at NLO

With the soft anomalous dimension matrices at hand, it is possible to calculate the infrared (IR) poles of the virtual amplitudes of the parton-parton $\to t\bar{t}j$ production process at NLO and compare them against the IR pole structure obtained using the Catani-Seymour subtraction formalism [45, 46].

In the Catani-Seymour formalism the expression for the NLO part of the NLO cross section reads

$$\delta\sigma_{\mathrm{NLO}} = \int_{n+1} [(d\sigma_{\mathrm{real}})_{\epsilon=0} + (dA)_{\epsilon=0}] + \int_n [d\sigma_{\mathrm{virt}} + \int_1 dA']_{\epsilon=0} + \int dx \int_n [d\sigma_{\mathrm{fact}} + dA'']_{\epsilon=0} , \quad (26)$$

with

$$0 = \int_{n+1} dA + \int_n \int_1 dA' + \int dx \int_n dA'' . \quad (27)$$

The terms dA, dA' and dA'' are constructed in such a way to make the individual integrands in Eq. (26) finite. dA represents the sum of all dipoles, $\int_1 dA'$ corresponds to the integral of the sum of all dipoles over the phase space of the additional soft and/or collinear parton causing divergences, i.e. the so-called **I**-term, and the term dA'' arises from mass factorization and includes the so-called **P**-, **K**- and **H**-terms.

All these terms are built using information about the soft and collinear factorization properties of QCD amplitudes. The subtraction term dA can be expressed as a sum of individual dipoles:

$$dA = \sum \mathcal{D}(i, j; k) . \quad (28)$$

This sum runs over all colored external partons in the scattering process. The possible $\{i, j; k\}$ combinations are obtained from the real corrections for which the subtraction term dA is constructed.

As an example let us consider the expression for $\mathcal{D}_{ij,k}(p_1, p_2, \ldots, p_{n+1})$:

$$\mathcal{D}_{ij,k}(p_1, p_2, \ldots, p_{n+1}) =$$
$$= -\frac{1}{2p_i \cdot p_j} \, {}_n\langle 1, \ldots \widetilde{ij}, \ldots, \tilde{k}, \ldots, n+1| \frac{\mathbf{T}_k \cdot \mathbf{T}_{ij}}{\mathbf{T}_{ij}^2} V_{ij,k} |1, \ldots \widetilde{ij}, \ldots, \tilde{k}, \ldots, n+1\rangle_n \,, \quad (29)$$

which describes the configuration corresponding to the splitting of a final-state parton $\widetilde{ij}$ (emitter) into the partons i and j in the presence of a final-state spectator parton $\tilde{k}$. The n-parton matrix element is obtained from the original $n + 1$-parton matrix element by replacing i and j with a single parton $\widetilde{ij}$ and k with $\tilde{k}$. In the previous equation, the color charge operator $\mathbf{T}_k$ is associated with the emission of a gluon from the parton k. If the emitted gluon has color index c, the color-charge operator is defined as

$$\mathbf{T}_k = \mathcal{T}_k^c |c\rangle \quad (30)$$

and its action onto the color space is defined by

$$\langle c_1, \ldots, c_k, \ldots c_m, c| \mathbf{T}_k |b_1, \ldots, b_k, \ldots b_m\rangle = \delta_{c_1 b_1} \ldots \mathcal{T}_{c_k b_k}^c \ldots \delta_{c_m b_m}, \quad (31)$$

where $\mathcal{T}_{cb}^a \equiv if_{cab}$ if the emitting parton k is a gluon (adjoint representation of the SU(N_c)), $\mathcal{T}_{cb}^a \equiv T_{cb}^a$ if the emitting parton is a quark (fundamental representation) and $\mathcal{T}_{cb}^a \equiv \overline{T}_{cb}^a$ $= -T_{bc}^a$ in case of an emitting antiquark[2]. These operators satisfy the usual color-algebra relations:

$$\mathbf{T}_k \cdot \mathbf{T}_j = \mathbf{T}_j \cdot \mathbf{T}_k \qquad \text{if} \quad k \neq j\,, \quad (32)$$
$$\mathbf{T}_k^2 = C_k \qquad \quad \forall\, k\,, \quad (33)$$

where $C_k = C_A$ for gluons and $C_k = C_F$ for quarks and antiquarks.

The matrix element

$${}_n\langle 1, \ldots \widetilde{ij}, \ldots, \tilde{k}, \ldots, n+1| \mathbf{T}_k \cdot \mathbf{T}_{ij} |1, \ldots \widetilde{ij}, \ldots, \tilde{k}, \ldots, n+1\rangle_n \quad (34)$$

is referred to in the literature as color linked Born amplitude squared (CLBS). The CLBS uses as input the reduced kinematics. The original momenta (p_i, p_j, p_k) are reduced to $(\tilde{p}_{ij}, \tilde{p}_k)$. In the dipole subtraction formalism the reduced kinematics obey the on-shell conditions and momentum conservation. This makes it possible to evaluate the CLBS

---

[2]Notice the difference in the color factor convention of the Catani-Seymour formalism with respect to the eikonal Feynman rules, as well as to the standard ones, where both quarks and antiquarks get color factors with a plus sign. This might seem inconsistent at a first glance, but actually it is not, keeping in mind that in case of the eikonal rules, the kinematic factor of the antiquark gets an extra minus sign with respect to the quark one. From the point of view of the sign, the factorization into a color and a kinematic factor is not unique and the minus sign can be assigned to either part. When using the results of calculation of soft anomalous dimension matrices in the dipole formalism through Eq. (35), it is important to remember the aforementioned aspects regarding the sign conventions.

analytically in a straightforward way or numerically by applying the existing codes for tree-level calculations. Notice that the color operators $\mathbf{T}_k \cdot \mathbf{T}_{ij}$ which enter the CLBS calculation, after bracketing, produce nothing else but the color factors also emerging from the calculation of the soft anomalous dimension matrices. Thus, the CLBS can be calculated as:

$$_n\langle 1, \ldots \widetilde{ij}, \ldots, \tilde{k}, \ldots, n+1 | \mathbf{T}_k \cdot \mathbf{T}_{ij} | 1, \ldots \widetilde{ij}, \ldots, \tilde{k}, \ldots, n+1 \rangle_n = \text{tr}(H_{AB}^{(0)} \tilde{\Gamma}_{BC}^{(1)}), \qquad (35)$$

where $H_{AB}^{(0)}$ are the components of the color decomposed Born-level hard-scattering amplitude and $\tilde{\Gamma}_{BC}^{(1)}$ are the color factors of the one loop soft anomalous dimension. $\tilde{\Gamma}_{BC}^{(1)}$ may differ from the color factor in the expression of $\Gamma_{BC}^{(1)}$ at most by an overall sign, cf. Footnote 2.

Using this formalism we evaluate the **I**-terms, which require the CLBS as input. The calculation of **I**, that was repeated for both the $q\bar{q}$- and the gg-induced subprocesses, was performed numerically using the automated tool `AutoDipole` [47]. The results obtained were then compared with **I**-terms calculated analytically using Eq. (35), where we inserted the $\tilde{\Gamma}^{(1)}$ matrix elements which are part of the $\Gamma^{(1)}$ ones presented in this work.

Additionally we verified that the matrix element of the **I** operator, calculated making use of Eq. (35), satisfies the following equation

$$_n\langle 1, \ldots \widetilde{ij}, \ldots, \tilde{k}, \ldots, n+1 | \mathbf{I} | 1, \ldots \widetilde{ij}, \ldots, \tilde{k}, \ldots, n+1 \rangle_n = \frac{C_{-2}}{\epsilon^2} + \frac{C_{-1}}{\epsilon} + C_0 \qquad (36)$$

producing the expected structure in terms of finite terms, simple and double poles and their coefficients.

All these calculations were automatized using `FORM` and the `SymPy` [48] library in the `python` module `pyDipole` [49]. This way we could confirm the correctness of all color factors of the soft anomalous dimension matrices and the validity of the color decomposition procedure.

6 Conclusions

Analytical expressions for all terms of the soft anomalous dimension matrices at one-loop for $t\bar{t}j$ production in parton-parton scattering close to threshold have been presented. This allows for the calculation of the one-loop soft functions, essential ingredients of the threshold factorization formula for the resummation of the logarithms associated to soft gluon emission at NLL accuracy. The expressions are provided in the most general axial gauge and have been subject to a number of analytical and numerical checks.

When the program of computing threshold resummation effects for the $t\bar{t}j$ hadroproduction process at NLO+NLL accuracy in QCD will be completed, indirect determinations of the top-quark mass with improved accuracy will indeed become possible, thus overcoming the limitations of previous extractions which have relied on NLO (or NLO+PS) differential distributions [50]. In particular, with the availability of results incorporating threshold

resummation effects, a much wider ρ_s interval will be accessible in the normalized ρ_s distribution with respect to the restricted one used so far. This increases the robustness of the extraction procedure and reduces the theoretical uncertainties on the extracted top-quark mass value. It is a crucial advancement of QCD theory in view of the high-statistics data foreseen for the High-Luminosity LHC phase and of the increase of competitiveness of indirect top-quark mass extractions with respect to the direct ones.

`FORM` files with the results for immediate use in resummation frameworks are also provided in ancillary files.

A   Color bases

We use the color bases of Ref. [39]. For completeness we list them below, with components in the same order in which they are used in the rest of our manuscript. In the following expressions for the basis elements, $\{T^e\}$ are the generators of the $\mathrm{SU}(N_c)$ group in the fundamental representation. They are $N_c \times N_c$ matrices. f^{emn} and d^{emn} are the totally antisymmetric and totally symmetric structure constants, obeying

$$
\begin{aligned}
f^{emn} &= 2i\mathrm{Tr}([T^e, T^m]T^n)\,, &(37)\\
d^{emn} &= 2\mathrm{Tr}(\{T^e, T^m\}T^n)\,, &(38)
\end{aligned}
$$

respectively. The color indices e, m, n run from 1 to $N_c^2 - 1$.

A.1   Color basis for $q_a\bar{q}_b \to q_c\bar{q}_d g_e$

$$
\begin{aligned}
(\mathbf{c}_1)_{abcde} &= \delta_{ab}T^e{}_{cd}\,,\\
(\mathbf{c}_2)_{abcde} &= \delta_{cd}T^e{}_{ba}\,,\\
(\mathbf{c}_3)_{abcde} &= T^m{}_{ba}T^n{}_{cd}if_{mne}\,,\\
(\mathbf{c}_4)_{abcde} &= T^m{}_{ba}T^n{}_{cd}d_{mne}\,,
\end{aligned}
\qquad (39)
$$

where the a, b, c, d color indices run from 1 to N_c and e, m, n run from 1 to $N_c^2 - 1$.

A.2 Color basis for $g_a g_b \to q_c \bar{q}_d g_e$

$$
\begin{aligned}
(\mathbf{c}_1)_{abcde} &= T^e{}_{cd}\delta_{ab}\,, \\
(\mathbf{c}_2)_{abcde} &= if_{abe}\delta_{cd}\,, \\
(\mathbf{c}_3)_{abcde} &= d_{abe}\delta_{cd}\,, \\
(\mathbf{c}_4)_{abcde} &= if_{abn}if_{men}T^m{}_{cd}\,, \\
(\mathbf{c}_5)_{abcde} &= d_{abn}if_{men}T^m{}_{cd}\,, \\
(\mathbf{c}_6)_{abcde} &= if_{abn}d_{men}T^m{}_{cd}\,, \\
(\mathbf{c}_7)_{abcde} &= d_{abn}d_{men}T^m{}_{cd}\,, \\
(\mathbf{c}_8)_{abcde} &= P^{10+\overline{10}}_{abme}T^m{}_{cd}\,, \\
(\mathbf{c}_9)_{abcde} &= P^{10-\overline{10}}_{abme}T^m{}_{cd}\,, \\
(\mathbf{c}_{10})_{abcde} &= -P^{27}_{abme}T^m{}_{cd}\,, \\
(\mathbf{c}_{11})_{abcde} &= P^{0}_{abme}T^m{}_{cd}\,,
\end{aligned}
\tag{40}
$$

where the c, d color indices run from 1 to N_c, the a, b, e, m, n color indices run from 1 to $N_c^2 - 1$, and the multiplet projectors are given as:

$$
\begin{aligned}
P^{0}_{abcd} &= -\frac{N d_{abg}d_{cdg}}{4(N-2)} - \frac{1}{2}f_{adg}f_{cbg} + \frac{1}{4}f_{abg}f_{cdg} \\
&\quad + \frac{1}{4}\delta_{ac}\delta_{bd} + \frac{1}{4}\delta_{ad}\delta_{cb} - \frac{\delta_{ab}\delta_{cd}}{2(N-1)}\,, \\
P^{10-\overline{10}}_{abcd} &= \frac{1}{2}d_{acg}if_{bgd} - \frac{1}{2}d_{bgd}if_{acg}\,, \\
P^{10+\overline{10}}_{abcd} &= \frac{1}{2}\left(\delta_{ac}\delta_{bd} - \delta_{ad}\delta_{cb}\right) - \frac{f_{abg}f_{cdg}}{N}\,, \\
P^{27}_{abcd} &= \frac{N d_{abg}d_{cdg}}{4(N+2)} + \frac{1}{2}f_{adg}f_{cbg} - \frac{1}{4}f_{abg}f_{cdg} + \frac{1}{4}\delta_{ad}\delta_{bc} \\
&\quad + \frac{1}{4}\delta_{ac}\delta_{bd} + \frac{\delta_{ab}\delta_{cd}}{2(N+1)}\,.
\end{aligned}
\tag{41}
$$

B A simple example of color decomposition

In this Appendix we show how the color decomposition can be done in the simplest cases, using as example the particular vertex correction graph depicted on the right-hand side of Fig. 2 among all those for the $q\bar{q} \to q\bar{q}g$ subprocess shown in Fig. 1a.

Following the argumentation of Ref. [39], one can use as Born-level color basis $\{\mathbf{c}_i\}$ the one in Appendix A.1, specifying the color indices to the case of the graph at hand (see
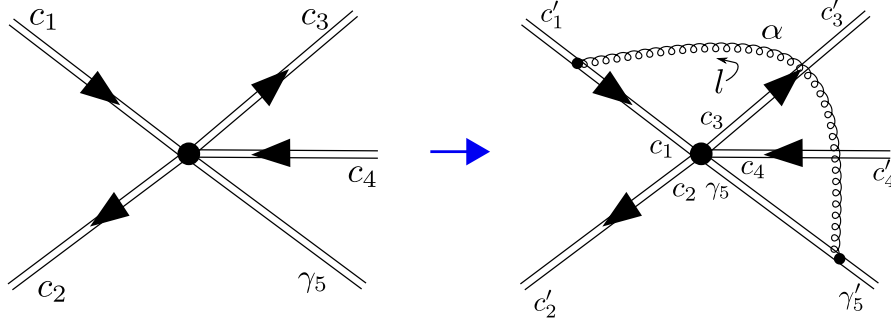
Figure 2: Example of color flow before and after soft gluon exchange.

Fig. 2):

$$\begin{aligned}
\mathbf{c}_1 &= \delta_{c_1 c_2} T^{\gamma_5}_{c_3 c_4}\,, \\
\mathbf{c}_2 &= \delta_{c_3 c_4} T^{\gamma_5}_{c_2 c_1}\,, \\
\mathbf{c}_3 &= T^{\alpha}_{c_2 c_1} T^{\beta}_{c_3 c_4} i f^{\alpha \beta \gamma_5}\,, \\
\mathbf{c}_4 &= T^{\alpha}_{c_2 c_1} T^{\beta}_{c_3 c_4} d^{\alpha \beta \gamma_5}\,,
\end{aligned} \tag{42}$$

with α, β, γ_5 running from 1 to $N_c^2 - 1$ and c_1, c_2, c_3, c_4 running from 1 to N_c. As shown in Fig. 2, the colors of two partons might change after a gluon exchange (e.g., for the case at hand, $c_1 \to c_1'$, $\gamma_5 \to \gamma_5'$). The basis in terms of color indices after gluon exchange $\{c_i'\}$ is then given by

$$\begin{aligned}
\mathbf{c}_1' &= \delta_{c_1' c_2'} T^{\gamma_5'}_{c_3' c_4'}\,, \\
\mathbf{c}_2' &= \delta_{c_3' c_4'} T^{\gamma_5}_{c_2' c_1'}\,, \\
\mathbf{c}_3' &= T^{\alpha}_{c_2' c_1'} T^{\beta}_{c_3' c_4'} i f^{\alpha \beta \gamma_5'}\,, \\
\mathbf{c}_4' &= T^{\alpha}_{c_2' c_1'} T^{\beta}_{c_3' c_4'} d^{\alpha \beta \gamma_5'}\,.
\end{aligned} \tag{43}$$

By performing color tensor manipulations, making use of the Fierz identity for the generators in the fundamental representation:

$$T^{\alpha}_{ij} T^{\alpha}_{kl} = \frac{1}{2}\left(\delta_{il}\delta_{jk} - \frac{1}{N_c}\delta_{ij}\delta_{kl} \right)\,, \tag{44}$$

and of the properties Eqs. (37) and (38) for the structure constants, one can show that the vertex correction leads to the following relation between the basis in terms of the Born-level color indices and the basis in terms of color indices after gluon exchange:

$$\mathbf{c}_1 \mathscr{F}_{15} = -\mathbf{c}_3'\,, \tag{45}$$

$$\mathbf{c}_2 \mathscr{F}_{15} = -\frac{N_c}{2}\mathbf{c}_2'\,, \tag{46}$$

$$\mathbf{c}_3 \mathscr{F}_{15} = -\frac{1}{2}\mathbf{c}_1' - \frac{N_c}{4}\mathbf{c}_3' - \frac{N_c}{4}\mathbf{c}_4'\,, \tag{47}$$

$$\mathbf{c}_4 \mathscr{F}_{15} = \left(\frac{1}{N_c} - \frac{N_c}{4} \right)\mathbf{c}_3' - \frac{N_c}{4}\mathbf{c}_4'\,. \tag{48}$$

We thus see that the linear transformation which describes the modification of the Born-color structure caused by the soft-gluon exchange between two partons (in this case incoming quark and outgoing gluon) is given by

$$\mathcal{F}_{15} = \begin{pmatrix} 0 & 0 & -\frac{1}{2} & 0 \\ 0 & -\frac{N_c}{2} & 0 & 0 \\ -1 & 0 & -\frac{N_c}{4} & \frac{1}{N_c} - \frac{N_c}{4} \\ 0 & 0 & -\frac{N_c}{4} & -\frac{N_c}{4} , \end{pmatrix} \tag{49}$$

which represents the color part of the soft anomalous dimension matrix. In other words, the matrices $\mathcal{F}_{ij}$ are defined such that:

$$\mathbf{c}\mathscr{F}_{ij} = \mathbf{c}'\mathcal{F}_{ij}, \tag{50}$$

where $\mathbf{c} = (\mathbf{c}_1, \mathbf{c}_2, \mathbf{c}_3, \mathbf{c}_4)$ and $\mathbf{c}' = (\mathbf{c}'_1, \mathbf{c}'_2, \mathbf{c}'_3, \mathbf{c}'_4)$.

The result presented in Eq. (49) coincides with the one already presented in Ref. [39], where one finds also the results for all other (i, j) pairs. In this way we calculated the $\mathcal{F}_{15}$ matrix for the graph shown, as well as those for other Wilson web graphs, as discussed in Sections 3 and 4.

References

[1] S. Alioli, P. Fernandez, J. Fuster, A. Irles, S. Moch, P. Uwer et al., *A new observable to measure the top-quark mass at hadron colliders*, *Eur. Phys. J. C* **73** (2013) 2438 [1303.6415].

[2] ATLAS collaboration, *Measurement of the top-quark mass in $t\bar{t}$ + 1-jet events collected with the ATLAS detector in pp collisions at $\sqrt{s} = 8$ TeV*, *JHEP* **11** (2019) 150 [1905.02302].

[3] CMS collaboration, *Determination of the normalised invariant mass distribution of $t\bar{t}$+jet and extraction of the top quark mass*, *CMS-PAS-TOP-13-006* (2016) .

[4] ATLAS collaboration, *Determination of the top-quark pole mass using tt t+1-jet events collected with the ATLAS experiment in 7 TeV pp collisions*, *ATLAS-CONF-2014-053* (2014) .

[5] ATLAS collaboration, *Determination of the top-quark pole mass using $t\bar{t}$ + 1-jet events collected with the ATLAS experiment in 7 TeV pp collisions*, *JHEP* **10** (2015) 121 [1507.01769].

[6] CMS collaboration, *Measurement of the top quark pole mass using $t\bar{t}$+jet events in the dilepton final state at $\sqrt{s} = 13$ TeV*, *CMS-PAS-TOP-21-008* (2022) .

[7] ATLAS collaboration, *Top quark mass summary plots March 2022*, *ATL-PHYS-PUB-2022-016* (2022) .

[8] U. Langenfeld, S. Moch and P. Uwer, *Measuring the running top-quark mass*, *Phys. Rev. D* **80** (2009) 054009 [0906.5273].

[9] A.H. Hoang, A. Jain, I. Scimemi and I.W. Stewart, *Infrared Renormalization Group Flow for Heavy Quark Masses*, *Phys. Rev. Lett.* **101** (2008) 151602 [0803.4214].

[10] A.H. Hoang, A. Jain, C. Lepenik, V. Mateu, M. Preisser, I. Scimemi et al., *The MSR mass and the $\mathcal{O}(\Lambda_{QCD})$ renormalon sum rule*, *JHEP* **04** (2018) 003 [1704.01580].

[11] M.V. Garzelli, L. Kemmler, S. Moch and O. Zenaiev, *Heavy-flavor hadro-production with heavy-quark masses renormalized in the $\overline{MS}$, MSR and on-shell schemes*, *JHEP* **04** (2021) 043 [2009.07763].

[12] S. Dittmaier, P. Uwer and S. Weinzierl, *NLO QCD corrections to $t\bar{t}$ + jet production at hadron colliders*, *Phys. Rev. Lett.* **98** (2007) 262002 [hep-ph/0703120].

[13] CMS collaboration, *Measurement of differential cross sections for the production of top quark pairs and of additional jets in pp collisions at* $\sqrt{s} = 13$ TeV, *CMS-PAS-TOP-20-006* (2022) .

[14] A. Kardos, C. Papadopoulos and Z. Trocsanyi, *Top quark pair production in association with a jet with NLO parton showering*, *Phys. Lett. B* **705** (2011) 76 [`1101.2672`].

[15] S. Alioli, S. Moch and P. Uwer, *Hadronic top-quark pair-production with one jet and parton showering*, *JHEP* **01** (2012) 137 [`1110.5251`].

[16] J. Alwall, R. Frederix, S. Frixione, V. Hirschi, F. Maltoni, O. Mattelaer et al., *The automated computation of tree-level and next-to-leading order differential cross sections, and their matching to parton shower simulations*, *JHEP* **07** (2014) 079 [`1405.0301`].

[17] M. Czakon, H.B. Hartanto, M. Kraus and M. Worek, *Matching the Nagy-Soper parton shower at next-to-leading order*, *JHEP* **06** (2015) 033 [`1502.00925`].

[18] C. Gütschow, J.M. Lindert and M. Schönherr, *Multi-jet merged top-pair production including electroweak corrections*, *Eur. Phys. J. C* **78** (2018) 317 [`1803.00950`].

[19] R. Frederix and S. Frixione, *Merging meets matching in MC@NLO*, *JHEP* **12** (2012) 061 [`1209.6215`].

[20] S. Badger, M. Becchetti, E. Chaubey, R. Marzucca and F. Sarandrea, *One-loop QCD helicity amplitudes for* $pp \to t\bar{t}j$ *to* $O(\epsilon^2)$, `2201.12188`.

[21] S. Catani and L. Trentadue, *Resummation of the QCD Perturbative Series for Hard Processes*, *Nucl. Phys. B* **327** (1989) 323.

[22] G.F. Sterman, *Summation of Large Corrections to Short Distance Hadronic Cross-Sections*, *Nucl. Phys. B* **281** (1987) 310.

[23] S. Moch, P. Uwer and A. Vogt, *On top-pair hadro-production at next-to-next-to-leading order*, *Phys. Lett. B* **714** (2012) 48 [`1203.6282`].

[24] M. Czakon and A. Mitov, *NNLO corrections to top-pair production at hadron colliders: the all-fermionic scattering channels*, *JHEP* **12** (2012) 054 [`1207.0236`].

[25] M. Czakon and A. Mitov, *NNLO corrections to top pair production at hadron colliders: the quark-gluon reaction*, *JHEP* **01** (2013) 080 [`1210.6832`].

[26] M. Czakon, P. Fiedler and A. Mitov, *Total Top-Quark Pair-Production Cross Section at Hadron Colliders Through* $O(\alpha_S^4)$, *Phys. Rev. Lett.* **110** (2013) 252004 [`1303.6254`].

[27] S. Catani, S. Devoto, M. Grazzini, S. Kallweit, J. Mazzitelli and H. Sargsyan, *Top-quark pair hadroproduction at next-to-next-to-leading order in QCD*, *Phys. Rev. D* **99** (2019) 051501 [`1901.04005`].

[28] N. Kidonakis, *Soft anomalous dimensions and resummation in QCD*, *Universe* **6** (2020) 165 [`2008.09914`].

[29] M. Sjodahl, *Color structure for soft gluon resummation: A General recipe*, *JHEP* **09** (2009) 087 [`0906.1121`].

[30] N. Agarwal, L. Magnea, C. Signorile-Signorile and A. Tripathi, *The Infrared Structure of Perturbative Gauge Theories*, `2112.07099`.

[31] N. Kidonakis, G. Oderda and G.F. Sterman, *Threshold resummation for dijet cross-sections*, *Nucl. Phys. B* **525** (1998) 299 [`hep-ph/9801268`].

[32] G. Sterman, *Mass divergences in annihilation processes. i. origin and nature of divergences in cut vacuum polarization diagrams*, *Phys. Rev. D* **17** (1978) 2773.

[33] N. Kidonakis and G.F. Sterman, *Resummation in heavy quark and jet cross-sections*, Frascati Phys. Ser. **5** (1996) 333 [`hep-ph/9607222`].

[34] J.C. Collins, D.E. Soper and G.F. Sterman, *Factorization for Short Distance Hadron - Hadron Scattering*, *Nucl. Phys. B* **261** (1985) 104.

[35] N. Kidonakis, G. Oderda and G.F. Sterman, *Evolution of color exchange in QCD hard scattering*, *Nucl. Phys. B* **531** (1998) 365 [`hep-ph/9803241`].

[36] J. Botts and G.F. Sterman, *Hard Elastic Scattering in QCD: Leading Behavior*, *Nucl. Phys. B* **325** (1989) 62.

[37] C.D. White, *An Introduction to Webs*, *J. Phys. G* **43** (2016) 033002 [`1507.02167`].

[38] N. Kidonakis and G.F. Sterman, *Resummation for QCD hard scattering*, *Nucl. Phys. B* **505** (1997) 321 [`hep-ph/9705234`].

[39] M. Sjodahl, *Color evolution of 2 → 3 processes*, *JHEP* **12** (2008) 083 [`0807.0555`].

[40] G. Leibbrandt, *Introduction to noncovariant gauges*, *Rev. Mod. Phys.* **59** (1987) 1067.

[41] J. Kuipers, T. Ueda, J.A.M. Vermaseren and J. Vollinga, *FORM version 4.0*, *Comput. Phys. Commun.* **184** (2013) 1453 [`1203.6543`].

[42] B. Chargeishvili, S. Moch and M.V. Garzelli, "FORMSoft - An automated tool for 1-loop soft anomalous dimension calculation." `https://git.bcharge.de/FORMSoft/`.

[43] B. Chargeishvili and S. Moch, "WilsonWebs - An automated tool for n-loop Wilson web generation." `https://git.bcharge.de/WilsonWebs/`.

[44] E. Szarek, *Soft anomalous dimension matrices in heavy quark-antiquark hadroproduction in association with a gluon jet*, *Acta Phys. Polon. B* **49** (2018) 1839 [`1809.00384`].

[45] S. Catani and M.H. Seymour, *A General algorithm for calculating jet cross-sections in NLO QCD*, *Nucl. Phys. B* **485** (1997) 291 [`hep-ph/9605323`].

[46] S. Catani, S. Dittmaier, M.H. Seymour and Z. Trocsanyi, *The Dipole formalism for next-to-leading order QCD calculations with massive partons*, *Nucl. Phys. B* **627** (2002) 189 [`hep-ph/0201036`].

[47] K. Hasegawa, S. Moch and P. Uwer, *AutoDipole: Automated generation of dipole subtraction terms*, *Comput. Phys. Commun.* **181** (2010) 1802 [`0911.4371`].

[48] A. Meurer et al., *Sympy: symbolic computing in python*, *PeerJ Computer Science* **3** (2017) e103.

[49] B. Chargeishvili, "pyDipole - A Python library for generating dipole subtraction terms." `https://git.bcharge.de/pyDipole/`.

[50] S. Alioli, J. Fuster, M.V. Garzelli, A. Gavardi, A. Irles, D. Melini et al., *Phenomenology of $t\bar{t}j + X$ production at the LHC*, *JHEP* **05** (2022) 146 [`2202.07975`].